Influence of Coulomb interaction on the anisotropic Dirac cone in graphene

Jing-Rong Wang[1,2] and Guo-Zhu Liu[1]

[1]*Department of Modern Physics, University of Science and Technology of China, Hefei, Anhui 230026, People's Republic of China*

[2]*Max Planck Institut für Physik komplexer Systeme, D-01187 Dresden, Germany*

(Received 6 November 2013; revised manuscript received 7 April 2014; published 5 May 2014)

Anisotropic Dirac cones can appear in a number of correlated electron systems, such as cuprate superconductors and deformed graphene. We study the influence of long-range Coulomb interaction on the physical properties of an anisotropic graphene by using the renormalization group method and $1/N$ expansion, where N is the flavor of Dirac fermions. Our explicit calculations reveal that the anisotropic fermion velocities flow monotonously to an isotropic fixed point in the lowest energy limit in clean graphene. We then incorporate three sorts of disorders, including random chemical potential, random gauge potential, and random mass, and show that the interplay of Coulomb interaction and disorders can lead to rich and unusual behaviors. In the presence of strong Coulomb interaction and a random chemical potential, the fermion velocities are driven to vanish at low energies and the system turns out to be an exotic anisotropic insulator. In the presence of Coulomb interaction and other two types of disorders, the system flows to an isotropic low-energy fixed point more rapidly than the clean case, and exhibits non-Fermi liquid behaviors. We also investigate the nonperturbative effects of Coulomb interaction, focusing on how the dynamical gap is affected by the velocity anisotropy. It is found that the dynamical gap is enhanced (suppressed) as the fermion velocities decrease (increase), but is suppressed as the velocity anisotropy increases.

DOI: 10.1103/PhysRevB.89.195404 PACS number(s): 71.10.Hf, 73.43.Nq, 74.62.En

I. INTRODUCTION

Massless Dirac fermions with a relativistic dispersion are known to be the low-energy elementary excitations in a variety of two-dimensional (2D) condensed matter systems, including d-wave superconductors [1,2], topological insulators [3], and graphene [4–9]. Different from the conventional Schrodinger electron systems with a finite Fermi surface, 2D Dirac fermion systems have discrete Fermi points and a vanishing density of states (DOS) at the lowest energy. Due to this difference, Dirac fermion systems exhibit nontrivial properties that cannot be realized in electron systems with a finite Fermi surface. These properties become particularly interesting when massless Dirac fermions couple to some kind of massless bosonic modes. For instance, Dirac fermions may interact strongly with a gauge field, a long-range Coulomb potential, or critical fluctuations of an order parameter, depending on the concrete materials.

If a Dirac fermion system has an isotropic Dirac cone, there will be a uniform fermion velocity v_F that can be defined from the kinetic energy $\varepsilon(k)$ by the relationship, $v_F \propto \partial\varepsilon(k)/\partial k|_{k_F}$. However, in many cases, the Dirac fermion systems may be spatially anisotropic for various reasons. A well-known example is the case of quasi-2D $d_{x^2-y^2}$-wave cuprate superconductors [1,2], where the massless nodal quasiparticles have a Fermi velocity v_F and a gap velocity v_Δ, obtained from the derivatives of the Fermi energy and superconducting gap, respectively. These two velocities are not equal in magnitude [2], and their ratio v_F/v_Δ can be as large as 10∼20. The velocity ratio is known to strongly affect many observable quantities [2]. Moreover, it is recently discovered that the isotropic Dirac cone of graphene can be made anisotropic once some external force, which might be uniaxial strain [10–13] or an external periodic potential [14–16], is applied to the originally ideal honeycomb lattice. When this happens, Dirac fermions have two different velocities, v_1 and v_2, with their ratio $\delta = v_2/v_1$ measuring the extent of spatial anisotropy. In addition, it is also possible to realize anisotropic Dirac cones in other Dirac fermion systems.

An interesting and widely studied problem is how the velocity anisotropy in Dirac fermion systems is affected by various interactions. We would like to know whether it is enhanced, weakened, or entirely suppressed. These problems deserve serious and systematic investigations for two reasons. First, the velocity ratio enters into many observable physical quantities, and hence should have measurable effects. Second, the interaction-induced nontrivial renormalization of velocity ratio can lead to a number of unusual behaviors. In the existing literature, the interactions of Dirac fermions with two sorts of critical bosonic excitations are broadly studied: gauge fields and order parameter fluctuations.

Gauge field. It has been proposed that much unusual physics of underdoped cuprates can be described by an effective QED_3 theory [1,17–21]. Within this effective theory, massless Dirac fermions couple strongly to an emergent U(1) gauge field, which may have different physical origins in different models [1,17–21]. Detailed renormalization group (RG) calculations have shown that gauge interaction drives the anisotropic fermion velocities to flow to an isotropic fixed point [18,21,22], i.e., $v_F/v_\Delta \to 1$. Therefore the velocity anisotropy is irrelevant, leading to a restored relativistic invariance [18].

Order parameter fluctuation. In the close vicinity of certain quantum phase transitions, massless Dirac fermions may couple to the fluctuation of some order parameters. For instance, the fermions interact with the fluctuation of a nematic order parameter at a nematic quantum critical point [23–29], which is supposed to exist in some d-wave superconductors. In contrast to the case of a gauge interaction, such interaction leads to an extreme anisotropy of fermion velocities [23,24], i.e., $v_\Delta/v_F \to 0$. Such an extreme anisotropy can give rise to a series of intriguing properties, such as non-Fermi liquid behavior [23,25], enhancement of thermal conductivity [26], and suppression of superconductivity [28]. Furthermore, Dirac

fermions may couple to an incommensurate antiferromagnetic order parameter. It was demonstrated [30] that this coupling is very similar to that between fermions and a nematic order parameter, so one could expect an analogous extreme anisotropy in this case.

In this paper, we further investigate the influence of strong interactions in anisotropic Dirac fermion systems. Here, we consider the long-range Coulomb interaction in a graphene that exhibits an anisotropic Dirac cone. RG techniques [31] will be used to address this issue. We are mainly interested in how the velocity ratio δ flows in the low-energy regime and how such flow affects the physical properties of the system.

Recently, the influence of Coulomb interaction on Dirac fermions with anisotropic dispersion is studied by Sharma *et. al.* [32], who have performed RG calculations by making perturbative expansion in powers of coupling constant $\alpha_1 = e^2/v_1\epsilon$, where v_1 is supposed to the larger component of the two velocities. It was argued [32] that Coulomb interaction can give rise to unusual behaviors. The RG scheme adopted in Ref. [32] could be improved in two important aspects. First, in the present problem, the Coulomb interaction strength is actually determined by both of the two components of fermion velocities, i.e., v_1 and v_2, hence the RG calculations performed by making expansion in powers of α_1 may not be able to capture all the essential features, especially when the anisotropy becomes strong. Second, the perturbative expansion in powers of coupling constant α_1 is valid only in the weak coupling regime, i.e., $\alpha_1 \ll 1$. However, the Coulomb interaction is known to play a much more significant role in the strong coupling regime, which cannot be accessed by the expansion scheme based on small α_1.

In order to perform a more general analysis that applies to both weak and strong couplings, here we will make use of the $1/N$-expansion method, with N being the flavor of Dirac fermions. This method proves to be powerful in dealing with field-theoretic models of strongly interacting fermionic systems. Although the physical fermion flavor is taken to be $N = 2$, to be explained in Sec. II, we will consider a general large N. An important advantage of this $1/N$-expansion method is that it can be straightforwardly generalized to include the nonperturbative effects of strong Coulomb interaction. After performing explicit RG calculations, we will show that both v_1 and v_2 increase monotonously with the decreasing energy and that the velocity ratio flows to unity, i.e., $v_2/v_1 \to 1$, in the lowest energy limit. Apparently, the anisotropic Dirac fermion system is driven to approach a stable isotropic fixed point at low energies by the Coulomb interaction.

It is also interesting to study the effects of quenched disorders, which exist in almost all realistic graphene samples and are known to govern many low-temperature transport properties [6,8,9]. The interactions between Dirac fermions and various disorders have recently stimulated extensive research works [33–36]. According to their coupling to Dirac fermions, disorders are usually divided into three classes: a random chemical potential, a random gauge potential, and random mass. We investigate the interplay of Coulomb interaction and fermion-disorder interaction, and demonstrate that it leads to a series of unusual behaviors, including the breakdown of Fermi liquid and emergence of non-Fermi liquid states. Further, it is shown that a random chemical potential exerts very different influence on the system compared with a random gauge potential and random mass. To understand these behaviors in more detail, we calculate the Landau damping rate, the DOS, and the specific heat after taking into account the effects of singular velocity renormalization and then discuss the physical properties of these quantities.

When the Coulomb interaction is sufficiently strong, a finite fermion gap may be dynamically generated through the formation of excitonic particle-hole pairs [37–48]. The dynamical gap generation drives an instability of the original semimetal ground state of graphene and leads to a semimetal-insulator quantum phase transition. Since the conventional perturbative expansion is unable to study this problem, we will combine the $1/N$ expansion with the Dyson-Schwinger (DS) gap equation methods, and then analyze the nonperturbative effects of strong Coulomb interaction. Our main interest here is the dependence of the dynamical gap generation on the fermion velocities and velocity ratio. In the presence of velocity anisotropy, the DS gap equation is formally very complicated. To simplify numerical computations, we introduce a number of approximations and try to extract some common feature from the numerical results. Our results show that the dynamical gap gets enhanced (suppressed) as the fermion velocities decrease (increase), whereas the dynamical gap is suppressed as the anisotropy increases.

The rest of the paper is organized as follows. In Sec. II, we write down the Hamiltonian and provide the Feynman rules that are used in the following calculations. Three sorts of disorders are introduced explicitly in this section. In Sec. III, we calculate the corrections to the self-energy function of fermions and the fermion-disorder vertex due to the interplay of Coulomb interaction and fermion-disorder interaction. We then derive the RG flow equations for fermion velocities and disorder strength parameters. In Sec. IV, we present numerical solutions of RG equations at four different limits and give a detailed interpretation of the results. In Sec. V, we compute a number of physical quantities after taking into account the velocity renormalization. In Sec. VI, we consider the effects of anisotropy on the dynamical gap generation after including the nonperturbative effects of Coulomb interaction. In Sec. VII, we summarize our results and discuss their physical implications.

II. MODEL HAMILTONIAN

After monolayer graphene was successfully separated in laboratories [4,5], a great deal of experimental and theoretical efforts have been devoted to explore its novel and fascinating properties [6,8,9]. Compared to the conventional metals, the most remarkable new feature of graphene is that its low-energy excitations are massless Dirac fermions having a linear dispersion. Since the fermion DOS vanishes at the neutral Dirac points, the Coulomb interaction between Dirac fermions remains long-ranged after including the dynamical screening due to particle-hole excitations. It is thus widely expected that such a long-range Coulomb interaction is responsible for many unusual behaviors of graphene [6,8,9].

The physical effects of Coulomb interaction have been extensively investigated, with those on fermion velocity renormalization [49–51], thermodynamics [52–54], and electric conductivity [35,55–62] being particularly intriguing. Here

we are mainly interested in the singular fermion velocity renormalization caused by the Coulomb interaction. If the Dirac cone is isotropic, the uniform velocity v_F will be strongly renormalized by Coulomb interaction, and driven to diverge in the lowest energy limit [49–51]. It is remarkable that the predicted singular renormalization of fermion velocity has already been observed in ultraclean suspended graphene [63], in graphene placed on a boron nitride (BN) substrate [64], and in ARPES measurements of quasi-free-standing graphene on silicon carbide (SiC) [65]. However, when graphene exhibits an anisotropic Dirac cone, the two components of fermion velocities should be renormalized separately. In this case, the velocity ratio may flow to some nontrivial fixed point.

We now write down the total Hamiltonian of the system. The free Hamiltonian of massless Dirac fermions with anisotropic dispersion is

$$H_0 = i\sum_{\sigma=1}^{N}\int d^2\mathbf{x}\bar{\Psi}_\sigma(\mathbf{x})\left[v_1\gamma_1\nabla_1 + v_2\gamma_2\nabla_2\right]\Psi_\sigma(\mathbf{x}), \quad (1)$$

where $\bar{\Psi} = \Psi^\dagger\gamma_0$. Here we have defined 4×4 matrices $\gamma_{0,1,2} = (\tau_3, -i\tau_2, i\tau_1)\otimes\tau_3$ in terms of Pauli matrices τ_i with $i = 1,2,3$, which satisfy the anticommutation relation $\{\gamma_\mu,\gamma_\nu\} = 2\mathrm{diag}(1,-1,-1)$. The spin index is σ, which takes all integers from 1 to N. The physical value of spin degeneracy is $N = 2$. However, to perform $1/N$ expansion, it is convenient to generalize the flavor to a large, general N. The two spatial components of the anisotropic fermion velocities are v_1 and v_2, respectively. The massless Dirac fermions couple to each other through the long-range Coulomb interaction

$$H_{\mathrm{ee}} = \frac{1}{4\pi}\sum_{\sigma,\sigma'=1}^{N}\int d^2\mathbf{x}d^2\mathbf{x}'\rho_\sigma(\mathbf{x})\frac{e^2}{\epsilon|\mathbf{x}-\mathbf{x}'|}\rho_{\sigma'}(\mathbf{x}'), \quad (2)$$

where $\rho_\sigma(\mathbf{x}) = \bar{\Psi}_\sigma(\mathbf{x})\gamma_0\Psi_\sigma(\mathbf{x})$ and ϵ is the dielectric constant whose magnitude is determined by the substrate.

The disorder scattering process can be described by coupling the Dirac fermions to a random field $A(\mathbf{x})$ in the following manner [34]:

$$H_{\mathrm{dis}} = v_\Gamma\sum_{\sigma=1}^{N}\int d^2\mathbf{x}\bar{\Psi}_\sigma(\mathbf{x})\Gamma\Psi_\sigma(\mathbf{x})A(\mathbf{x}). \quad (3)$$

The random field $A(\mathbf{x})$ is a quenched Gaussian variable, which satisfies

$$\langle A(\mathbf{x})\rangle = 0, \quad \langle A(\mathbf{x})A(\mathbf{x}')\rangle = \Delta\delta^2(\mathbf{x}-\mathbf{x}'), \quad (4)$$

where Δ is a dimensionless variance. Here, we consider three types of disorders distinguished by the definitions of the Γ matrix [34]. More concretely, $\Gamma = \gamma_0$ for a random chemical potential, $\Gamma = (\gamma_1,\gamma_2)$ and $v_\Gamma = (v_{\Gamma 1}, v_{\Gamma 2})$ for a random gauge potential, and $\Gamma = \mathbb{1}_{4\times 4}$ for random mass. Physically, a random chemical potential may be induced by local defects, neutral impurity atoms or neutral absorbed atoms in the plane of graphene [7,66]; a random gauge field can be generated by ripples of graphene [6,35,36,67]; random mass may be produced by the random configurations of the substrates [68,69].

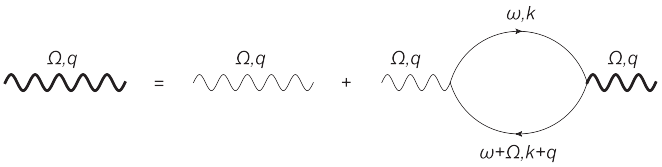

FIG. 1. One-loop Feynman diagram for dynamical screening of Coulomb interaction, where the solid line represents the free propagator of Dirac fermions, the thin wavy line represents the bare Coulomb interaction function, and the thick wavy line represents the dynamically screened Coulomb interaction function.

Starting from H_0, it is easy to obtain the free Dirac fermion propagator

$$G_0(i\omega,\mathbf{k}) = \frac{1}{-i\omega\gamma_0 + v_1k_1\gamma_1 + v_2k_2\gamma_2}. \quad (5)$$

The bare Coulomb interaction is

$$D_0(q) = \frac{2\pi e^2}{\epsilon|\mathbf{q}|}. \quad (6)$$

At the one-loop level, the polarization is given by

$$\begin{aligned}\Pi(i\Omega,\mathbf{q}) &= -N\int\frac{d\omega}{2\pi}\frac{d^2\mathbf{k}}{(2\pi)^2}\mathrm{Tr}\left[\gamma_0G_0(i\omega,\mathbf{k})\gamma_0\right.\\ &\quad\left.\times G_0(i\omega+i\Omega,\mathbf{k}+\mathbf{q})\right]\\ &= \frac{N}{8v_1v_2}\frac{v_1^2q_1^2+v_2^2q_2^2}{\sqrt{\Omega^2+v_1^2q_1^2+v_2^2q_2^2}}. \quad (7)\end{aligned}$$

It is consistent with the polarization obtained by Sharma *et al.* [32]. It is shown perviously [70,71] that the polarization in strained graphene is related to the polarization in unstrained graphene by an additional prefactor and a linear transformation for the momenta. Here, the polarization is calculated by starting directly from a fermion propagator with an anisotropic dispersion, namely Eq. (5). The polarization obtained in Refs. [70,71] is basically equivalent to Eq. (7) at the zero chemical potential limit.

According to the diagram shown in Fig. 1, the dressed Coulomb interaction should be written as

$$D^{-1}(i\Omega,\mathbf{q}) = \frac{\epsilon|\mathbf{q}|}{2\pi e^2} + \frac{N}{8v_1v_2}\frac{v_1^2q_1^2+v_2^2q_2^2}{\sqrt{\Omega^2+v_1^2q_1^2+v_2^2q_2^2}}. \quad (8)$$

In the isotropic case, $v_1 = v_2 = v$, hence the strength of Coulomb interaction can be well described by a single parameter $\alpha = e^2/v\epsilon$. In the anisotropic case, however, the Coulomb interaction is actually characterized by two parameters, i.e., the coupling $\alpha_1 = e^2/v_1\epsilon$ and the velocity ratio $\delta = v_2/v_1$. Therefore, at any given coupling α_1, the effective interaction strength is changing as one tunes the ratio δ.

III. RENORMALIZATION GROUP ANALYSIS TO THE LEADING ORDER OF $1/N$ EXPANSION

In this section, we first calculate the self-energy corrections of Dirac fermions caused by the interplay of Coulomb interaction and disorder scattering, and then calculate the corrections

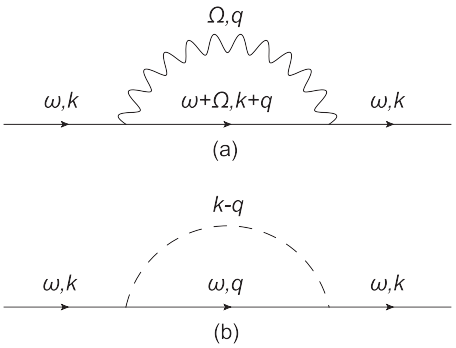

FIG. 2. Fermion self-energy correction due to (a) Coulomb interaction and (b) disorder. The dashed line represents disorder scattering.

to the fermion-disorder vertex. On the basis of these results, we will be able to derive the analytical expressions of RG flow equations for fermion velocities and disorder strength parameters. Our calculations are done to the leading order of $1/N$ expansion.

A. Fermion self-energy and vertex correction

The Dirac fermions receive self-energy corrections from both the Coulomb interaction and the fermion-disorder interaction, described by the diagrams shown in Fig. 2. According to Fig. 2(a), the fermion self-energy due to Coulomb interaction is given by

$$\Sigma_C(i\omega,\mathbf{k}) = -\int \frac{d^2\mathbf{q}}{(2\pi)^2}\int \frac{d\Omega}{2\pi}\gamma_0 G_0(i\Omega+i\omega,\mathbf{q}+\mathbf{k})\gamma_0 \times D(i\Omega,\mathbf{q}). \quad (9)$$

After substituting Eqs. (5) and (8) into this expression and performing tedious analytical calculations, which are detailed in Appendix A, we obtain

$$\frac{d\Sigma_C(i\omega,\mathbf{k})}{d\ln\Lambda} = -i\omega\gamma_0 C_0 + v_1 k_1\gamma_1 C_1 + v_2 k_2\gamma_2 C_2, \quad (10)$$

where

$$C_0 = \frac{1}{8\pi^3}\int_{-\infty}^{+\infty} dx\int_0^{2\pi} d\theta \times \frac{-x^2+\cos^2\theta+(v_2/v_1)^2\sin^2\theta}{[x^2+\cos^2\theta+(v_2/v_1)^2\sin^2\theta]^2}\mathcal{G}(x,\theta), \quad (11)$$

$$C_1 = \frac{1}{8\pi^3}\int_{-\infty}^{+\infty} dx\int_0^{2\pi} d\theta \times \frac{-x^2+\cos^2\theta-(v_2/v_1)^2\sin^2\theta}{[x^2+\cos^2\theta+(v_2/v_1)^2\sin^2\theta]^2}\mathcal{G}(x,\theta), \quad (12)$$

$$C_2 = \frac{1}{8\pi^3}\int_{-\infty}^{+\infty} dx\int_0^{2\pi} d\theta \times \frac{-x^2-\cos^2\theta+(v_2/v_1)^2\sin^2\theta}{[x^2+\cos^2\theta+(v_2/v_1)^2\sin^2\theta]^2}\mathcal{G}(x,\theta), \quad (13)$$

and

$$\mathcal{G}^{-1}(x,\theta) = \frac{1}{2\pi\alpha_1} + \frac{N}{8v_2/v_1}\frac{\cos^2\theta+(v_2/v_1)^2\sin^2\theta}{\sqrt{x^2+\cos^2\theta+(v_2/v_1)^2\sin^2\theta}} \quad (14)$$

with $\alpha_1 = \frac{e^2}{v_1\epsilon}$. Here, we point out that Eqs. (11)–(14) can also be written in the symmetric forms presented in Appendix C. In order to directly compare our results to those obtained based on a perturbative expansion in powers of α_1 [32,72], we will use the nonsymmetric expressions of $C_{0,1,2}$ and $\mathcal{G}$.

According to Fig. 2(b), the fermion self-energy induced by disorder takes the form

$$\Sigma_{\rm dis}(i\omega) = \Delta v_\Gamma^2\int\frac{d^2\mathbf{q}}{(2\pi)^2}\Gamma G_0(i\omega,\mathbf{q})\Gamma = i\omega v_\Gamma^2\Delta\int\frac{d^2\mathbf{q}}{(2\pi)^2}\frac{\Gamma\gamma_0\Gamma}{\left(\omega^2+v_1^2q_1^2+v_2^2q_2^2\right)}. \quad (15)$$

Different from the case of the Coulomb interaction, $\Sigma_{\rm dis}(i\omega)$ is independent of momentum, which reflects the fact that disorders are static. We now have

$$\frac{d\Sigma_{\rm dis}(i\omega)}{d\ln\Lambda} = C_g i\omega\gamma_0, \quad (16)$$

where

$$C_g = \frac{v_\Gamma^2\Delta}{2\pi v_1 v_2} \quad (17)$$

for a random chemical potential and random mass, and

$$C_g = \frac{\left(v_{\Gamma1}^2+v_{\Gamma2}^2\right)\Delta}{2\pi v_1 v_2} \quad (18)$$

for a random gauge potential.

We next consider the corrections to the fermion-disorder vertex, which receives contributions from both Coulomb interaction and fermion-disorder interaction, as described by the diagrams shown in Fig. 3. According to Fig. 3(a), at zero

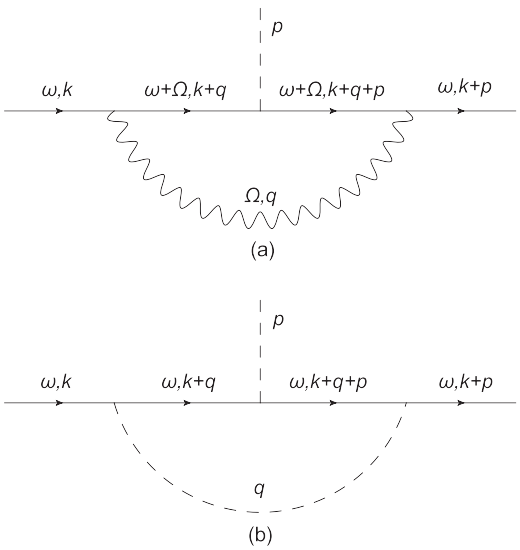

FIG. 3. Fermion-disorder vertex correction due to (a) Coulomb interaction and (b) disorder.

external momentum and frequency, the vertex correction due to Coulomb interaction is calculated as follows:

$$V_C = -\int \frac{d\Omega}{2\pi}\int \frac{d^2\mathbf{q}}{(2\pi)^2}\gamma_0 G_0(i\Omega,\mathbf{q})v_\Gamma\Gamma G_0(i\Omega,\mathbf{q})\gamma_0 \times D(i\Omega,\mathbf{q}). \quad (19)$$

After analytical calculations detailed in Appendix B, we have

$$\frac{dV_C}{d\ln\Lambda} = v_\Gamma\gamma_0(-C_0) \quad (20)$$

for a random chemical potential,

$$\frac{dV_C}{d\ln\Lambda} = v_{\Gamma 1}\gamma_1(-C_1), \quad (21)$$

$$\frac{dV_C}{d\ln\Lambda} = v_{\Gamma 2}\gamma_2(-C_2) \quad (22)$$

for the γ_1 and γ_2 components of a random gauge potential, respectively, and

$$\frac{dV_C}{d\ln\Lambda} = v_\Gamma\mathbb{1}(C_0 - C_1 - C_2) \quad (23)$$

for random mass.

According to Fig. 3(b), at zero momentum, the vertex correction due to averaging over disorders is found to be

$$V_{\rm dis} = \Delta v_\Gamma^2\int \frac{d^2\mathbf{q}}{(2\pi)^2}\Gamma G_0(i\omega,\mathbf{q})v_\Gamma\Gamma G_0(i\omega,\mathbf{q})\Gamma. \quad (24)$$

It is shown that

$$\frac{dV_{\rm dis}}{d\ln\Lambda} = v_\Gamma\gamma_0 C_g \quad (25)$$

for a random chemical potential,

$$\frac{dV_{\rm dis}}{d\ln\Lambda} = 0 \quad (26)$$

for a random gauge potential, and

$$\frac{dV_{\rm dis}}{d\ln\Lambda} = -v_\Gamma\mathbb{1}C_g \quad (27)$$

for random mass.

B. Derivation of the RG equations

The fermion self-energy corrections and fermion-disorder corrections obtained in the last section will be used to derive the relevant RG equations. According to the renormalization group theory [24,27,31], after integrating out the fields in the momentum shell $\Lambda/b < k < \Lambda$ with $b > 1$, where b can be written as $b = e^l$ with a running scale $l > 0$, we can get the following action for the fermion:

$$\begin{aligned} S_\Psi &= \sum_{\sigma=1}^{N}\int\frac{d\omega}{2\pi}\frac{d^2\mathbf{k}}{(2\pi)^2}\bar\Psi_\sigma(i\omega,\mathbf{k})\big[G_0^{-1}(i\omega,\mathbf{k}) - \Sigma_C(i\omega,\mathbf{k}) \\ &\quad - \Sigma_{\rm dis}(i\omega,\mathbf{k})\big]\Psi_\sigma(i\omega,\mathbf{k}), \\ &\approx \sum_{\sigma=1}^{N}\int\frac{d\omega}{2\pi}\frac{d^2\mathbf{k}}{(2\pi)^2}\bar\Psi_\sigma(i\omega,\mathbf{k})\big[-i\omega\gamma_0 e^{\int_0^l dl(-C_0+C_g)} \\ &\quad + v_1k_1e^{\int_0^l dl(-C_1)} + v_2k_2e^{\int_0^l dl(-C_2)}\big]\Psi_\sigma(i\omega,\mathbf{k}). \end{aligned} \quad (28)$$

In the spirit of RG theory [24,27,31], one can perform the following rescaling transformation:

$$k_i = k_i'e^{-l}, \quad (29)$$

$$\omega = \omega'e^{-l}, \quad (30)$$

$$\Psi_\sigma(i\omega,\mathbf{k}) = \Psi_\sigma'(i\omega',\mathbf{k}')e^{\frac{1}{2}\int_0^l dl(4+C_0-C_g)}, \quad (31)$$

$$v_1 = v_1'e^{\int_0^l dl(-C_0+C_1+C_g)}, \quad (32)$$

$$v_2 = v_2'e^{\int_0^l dl(-C_0+C_2+C_g)}, \quad (33)$$

which should keep the kinetic term of fermions invariant, namely

$$\begin{aligned} S_{\Psi'} &= \sum_{\sigma=1}^{N}\int\frac{d\omega'}{2\pi}\frac{d^2\mathbf{k}'}{(2\pi)^2}\bar\Psi_\sigma'(i\omega',\mathbf{k}')[-i\omega'\gamma_0 + v_1'k_1' \\ &\quad + v_2'k_2']\Psi_\sigma'(i\omega',\mathbf{k}'). \end{aligned} \quad (34)$$

After including the influence of interaction, the action for the disorder scattering to the fermion becomes

$$\begin{aligned} S_{\rm dis} &= \sum_{\sigma=1}^{N}\int\frac{d\omega}{2\pi}\frac{d^2\mathbf{k}}{(2\pi)^2}\int\frac{d^2\mathbf{k}_1}{(2\pi)^2}\bar\Psi_\sigma(i\omega,\mathbf{k})(\Gamma + V_C \\ &\quad + V_{\rm dis})\Psi_\sigma(i\omega,\mathbf{k}_1)A(\mathbf{k}-\mathbf{k}_1). \end{aligned} \quad (35)$$

Specifically,

$$\begin{aligned} S_{\rm dis} &\approx \sum_{\sigma=1}^{N}\int\frac{d\omega}{2\pi}\frac{d^2\mathbf{k}}{(2\pi)^2}\int\frac{d^2\mathbf{k}_1}{(2\pi)^2}\bar\Psi_\sigma(i\omega,\mathbf{k})v_\Gamma\gamma_0 \\ &\quad \times e^{\int_0^l dl(-C_0+C_g)}\Psi_\sigma(i\omega,\mathbf{k}_1)A(\mathbf{k}-\mathbf{k}_1) \end{aligned} \quad (36)$$

for a random chemical potential,

$$\begin{aligned} S_{\rm dis} &\approx \sum_{\sigma=1}^{N}\int\frac{d\omega}{2\pi}\frac{d^2\mathbf{k}}{(2\pi)^2}\int\frac{d^2\mathbf{k}_1}{(2\pi)^2}\bar\Psi_\sigma(i\omega,\mathbf{k})v_\Gamma\gamma_1 \\ &\quad \times e^{\int_0^l dl(-C_1)}\Psi_\sigma(i\omega,\mathbf{k}_1)A(\mathbf{k}-\mathbf{k}_1), \end{aligned} \quad (37)$$

$$\begin{aligned} S_{\rm dis} &\approx \sum_{\sigma=1}^{N}\int\frac{d\omega}{2\pi}\frac{d^2\mathbf{k}}{(2\pi)^2}\int\frac{d^2\mathbf{k}_1}{(2\pi)^2}\bar\Psi_\sigma(i\omega,\mathbf{k})v_\Gamma\gamma_2 \\ &\quad \times e^{\int_0^l dl(-C_2)}\Psi_\sigma(i\omega,\mathbf{k}_1)A(\mathbf{k}-\mathbf{k}_1) \end{aligned} \quad (38)$$

for the γ_1 and γ_2 components of a random gauge potential, respectively, and

$$\begin{aligned} S_{\rm dis} &= \sum_{\sigma=1}^{N}\int\frac{d\omega}{2\pi}\frac{d^2\mathbf{k}}{(2\pi)^2}\int\frac{d^2\mathbf{k}_1}{(2\pi)^2}\bar\Psi_\sigma(i\omega,\mathbf{k})v_\Gamma\mathbb{1} \\ &\quad \times e^{\int_0^l dl(C_0-C_1-C_2-C_g)}\Psi_\sigma(i\omega,\mathbf{k}_1)A(\mathbf{k}-\mathbf{k}_1) \end{aligned} \quad (39)$$

for the random mass. Carry out the scaling (29)–(31) along with

$$A(\mathbf{k}) = A'(\mathbf{k}')e^l, \quad (40)$$

and

$$v_\Gamma = v_\Gamma' \quad (41)$$

for a random chemical potential,

$$v_{\Gamma 1} = v'_{\Gamma 1} e^{\int_0^l dl(-C_0+C_1+C_g)}, \tag{42}$$

$$v_{\Gamma 2} = v'_{\Gamma 2} e^{\int_0^l dl(-C_0+C_2+C_g)} \tag{43}$$

for the γ_1 and γ_2 components of a random gauge potential, respectively, and

$$v_{\Gamma} = v'_{\Gamma} e^{\int_0^l dl(-2C_0+C_1+C_2+2C_g)} \tag{44}$$

for random mass. Then the corresponding action can keep the invariant form as

$$S_{\rm dis} = \sum_{\sigma=1}^{N} \int \frac{d\omega'}{2\pi} \frac{d^2\mathbf{k}'}{(2\pi)^2} \int \frac{d^2\mathbf{k}'_1}{(2\pi)^2} \bar{\Psi}'_\sigma(i\omega',\mathbf{k}') v'_\Gamma \Gamma \times \Psi'_\sigma(i\omega',\mathbf{k}'_1) A'(\mathbf{k}'-\mathbf{k}'_1). \tag{45}$$

From Eqs. (32), (33), (41)–(44), we can get the renormalization group equations:

$$\frac{dv_1}{dl} = (C_0 - C_1 - C_g) v_1, \tag{46}$$

$$\frac{dv_2}{dl} = (C_0 - C_2 - C_g) v_2, \tag{47}$$

$$\frac{d(v_2/v_1)}{dl} = (C_1 - C_2) \frac{v_2}{v_1}, \tag{48}$$

and

$$\frac{dv_\Gamma}{dl} = 0 \tag{49}$$

for a random chemical potential,

$$\frac{dv_{\Gamma 1}}{dl} = (C_0 - C_1 - C_g) v_{\Gamma 1}, \tag{50}$$

$$\frac{dv_{\Gamma 2}}{dl} = (C_0 - C_2 - C_g) v_{\Gamma 2} \tag{51}$$

for the γ_1 and γ_2 components of a random gauge potential, respectively,

$$\frac{dv_\Gamma}{dl} = (2C_0 - C_1 - C_2 - 2C_g) v_\Gamma \tag{52}$$

for random mass.

IV. NUMERICAL RESULTS

In this section, we present numerical solutions of RG equations obtained in Sec. III and discuss their physical implications. In order to examine the effects of various physical mechanisms and parameters, it is helpful to analyze the results at different limits. First, we consider the case of an isotropic Dirac cone in the absence of disorders. Second, we consider the case of an anisotropic Dirac cone in the absence of disorders. Third, we consider an isotropic Dirac cone in the presence of disorders. Finally, we turn to the anisotropic Dirac cone in the presence of disorders.

A. Clean isotropic case

We first consider graphene with isotropic Dirac cones and uniform velocity, $v_1 = v_2 = v$, and assume the sample is clean.

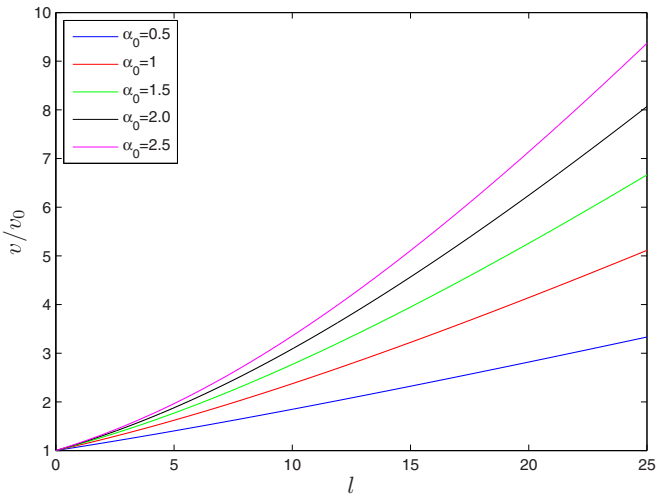

FIG. 4. (Color online) Renormalized fermion velocity for isotropic Dirac cone and without disorder.

In this case, the velocity flows as

$$\frac{dv}{dl} = Cv, \tag{53}$$

where

$$C = \frac{4}{N\pi^2}\left[1 - \frac{1}{\lambda}\frac{\pi}{2} + \frac{1}{\lambda}\begin{cases} \frac{1}{\sqrt{1-\lambda^2}}\arccos(\lambda) & \lambda < 1 \\ \frac{1}{\sqrt{\lambda^2-1}}\operatorname{arccosh}(\lambda) & \lambda > 1 \\ 1 & \lambda = 1 \end{cases}\right]$$

with $\lambda = \frac{N\pi\alpha}{4}$. This result has previously been obtained by Son [51]. The renormalized fermion velocity, shown in Fig. 4, increases monotonically in the low-energy regime. It is interesting that this behavior is recently observed in experiments [63–65].

B. Clean anisotropic case

We then consider clean graphene with an anisotropic Dirac cone. We obtain the following flow equations of fermion velocities $v_{1,2}$ and their ratio:

$$\frac{dv_1}{dl} = (C_0 - C_1) v_1, \tag{54}$$

$$\frac{dv_2}{dl} = (C_0 - C_2) v_2, \tag{55}$$

$$\frac{d(v_2/v_1)}{dl} = (C_1 - C_2) \frac{v_2}{v_1}, \tag{56}$$

where $C_{0,1,2}$ are given in Sec. III. From Fig. 5, it is easy to see that both v_1 and v_2 increase monotonically with the decreasing energy scale, and that the velocities flow to the isotropic limit at the lowest energy, i.e., $v_2/v_1 \to 1$ as $l \to \infty$. Apparently, the velocity anisotropy is irrelevant, analogous to the case of QED_3 [18,21,22]. Notice this conclusion is different from the nonmonotonic flow of velocity ratio claimed in Ref. [32].

It is now necessary to make a comparison between our results and those of Ref. [32]. Sharma *et. al.* investigated the influence of Coulomb interaction on Dirac fermion systems with an anisotropic dispersion by performing a perturbative

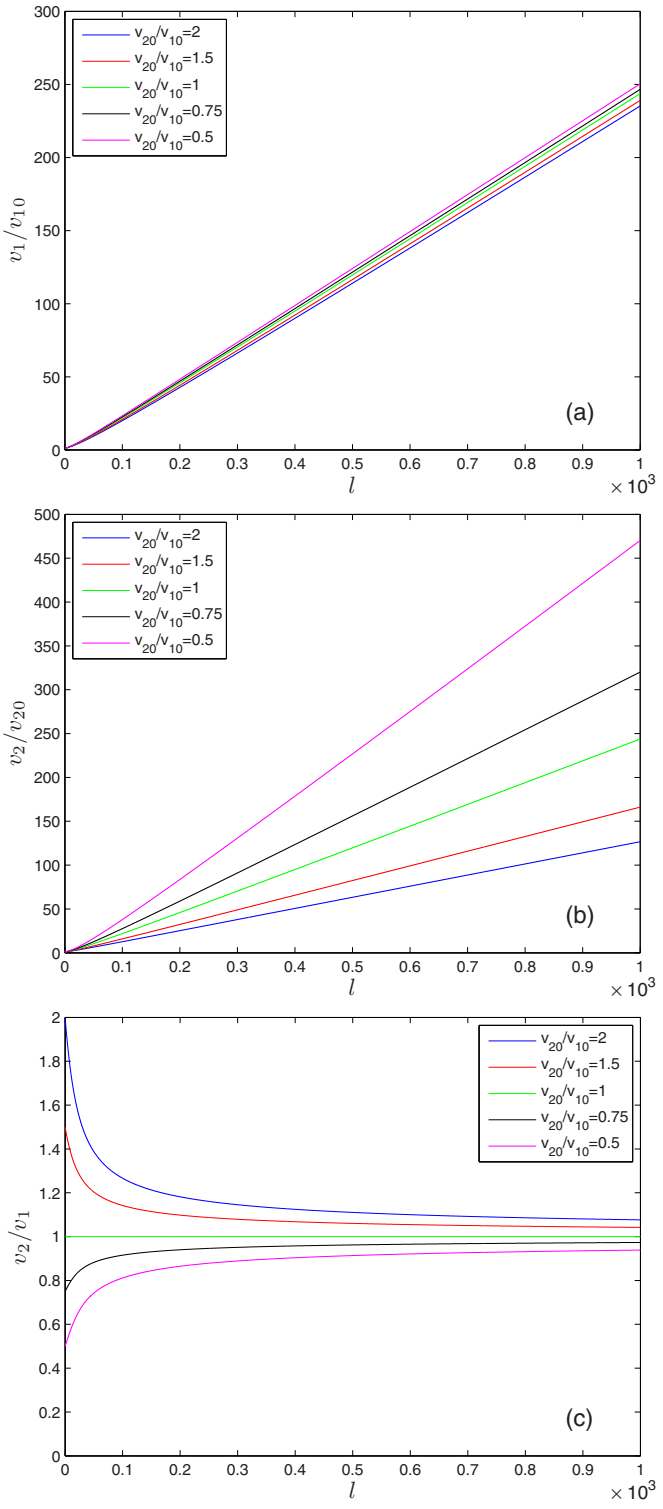

FIG. 5. (Color online) Renormalized v_1, v_2, and v_2/v_1 at fixed coupling $\alpha_{10} = e^2/\epsilon v_{10} = 1$ in the absence of disorders.

expansion in powers of $\alpha_1 = e^2/v_1\epsilon$ [32]. They found that the system will flow to three different fixed points, depending on the initial values of α_1 and $\delta = v_2/v_1 - 1$ (notice that the meaning of δ in our paper is different from Ref. [32]), where it is assumed that $v_2 < v_1$ with $\delta = -1$ representing an infinite anisotropic limit. When α_1 is small and $|\delta|$ is smaller than a certain critical value, the flow of δ is not monotonic. In particular, the anisotropy of fermion dispersion initially increases with decreasing energy in a range of energy scale, but finally goes to an isotopic limit at the lowest energy. If α_1 is strong enough, the system can become an anisotropic insulator. If α_1 is small and $|\delta|$ is larger than a certain critical value, the system will become a quasi-one-dimensional non-Fermi liquid. It is obvious that these results differ significantly from ours.

We would point out that the perturbative expansion presented in Ref. [32] is valid if the Coulomb interaction is weak. This expansion scheme is no longer valid when the Coulomb interaction becomes strong. In addition, the Coulomb interaction strength actually depends on both α_1 and δ. Since δ itself also flows strongly with the varying energy, it seems questionable to make a perturbative expansion in powers of α_1 alone. In order to avoid these problems and make the RG analysis reliable for both weak and strong couplings, we have chosen to study the influence of Coulomb interaction on velocity anisotropy by means of the $1/N$ expansion. As demonstrated in our results, the anisotropic system flows to an isotropic fixed point. An earlier calculation of Aleiner *et al.* has showed that the long-range Coulomb interaction tends to suppress the strength of a trigonal wrapping term, which otherwise can make the system anisotropic [73]. Our conclusion, though based on a different approach, agrees with that of Ref. [73].

When the Coulomb interaction becomes sufficiently strong, the perturbative $1/N$ expansion is also invalid since the interaction may lead to an excitonic instability. We do agree with Ref. [32] on the opinion that the excitonic insulating transition should be investigated by means of a nonperturbative method. This issue will be addressed in Sec. VI by constructing and solving the self-consistent DS gap equation.

C. Disordered and isotropic case

Now we come to the case of an isotropic Dirac cone in the presence of disorders. After assuming $v_1 = v_2 = v$ and introducing disordered potentials, we find that

$$\frac{dv}{dl} = (C - C_g)v, \tag{57}$$

and that

$$\frac{dv_\Gamma}{dl} = 0 \tag{58}$$

for a random chemical potential,

$$\frac{dv_\Gamma}{dl} = (C - C_g)v_\Gamma \tag{59}$$

for a random gauge potential, and

$$\frac{dv_\Gamma}{dl} = 2(C - C_g)v_\Gamma \tag{60}$$

for random mass. Apparently, the flows of v_Γ in a random gauge potential and random mass are very similar, but are quite different from a random chemical potential.

The fixed point α^* for a random chemical potential, a random gauge potential, and random mass can be obtained

by setting

$$C(\alpha^*) - C_g(\alpha^*) = 0. \tag{61}$$

The expression of C as a function of α is presented in Sec. IV A. As will be shown in Eqs. (63), (65), and (67), C_g can also be written as a function of α, in different forms for different kinds of disorders. This issue has been studied earlier by Stauber *et al.* [34], who have made perturbative expansions in powers of interaction strength. It was discovered in Ref. [34] that $\alpha^* \propto \Delta^{-1}$ for a random chemical potential, $\alpha^* \propto \Delta$ for a random gauge potential, and $\alpha^* \propto \Delta^3$ for random mass. Our calculations are performed by means of a $1/N$ expansion approach and have reached quantitatively different results, depicted in Fig. 6. However, in agreement with the qualitative results of Stauber *et al.* [34], we find that the fixed points for both a random gauge potential and random mass are stable, whereas there is no stable fixed point for a random chemical potential. We now present our results for a random chemical potential, a random gauge potential, and random mass, respectively, in order.

For a random chemical potential, Eq. (58) implies that

$$v_\Gamma = v_{\Gamma 0}, \tag{62}$$

then C_g can be written as the function of α:

$$C_g = \frac{v_\Gamma^2 \Delta}{2\pi v^2} = \frac{v_{\Gamma 0}^2 \Delta}{2\pi v^2} = \left(\frac{v_{\Gamma 0}^2 \Delta \epsilon^2}{2\pi e^4}\right)\alpha^2. \tag{63}$$

The lines of fixed points are shown in Fig. 6(a). Apparently, the fixed points are unstable in this case. Figure 7(a) shows the velocity flow at different values of α_0. If α_0 is smaller than some critical value $\alpha^*(\Delta)$, the velocity increases continuously as the energy scale is decreasing, and the effective strength of Coulomb interaction flows to the infinitely weak coupling limit. In this case, the weak Coulomb interaction is obviously irrelevant. However, when $\alpha_0 > \alpha^*(\Delta)$, the fermion velocity decreases with decreasing energy scale, and finally vanishes at certain finite energy scale, which means the effective strength of Coulomb interaction is greatly enhanced and flows to an infinitely strong coupling limit before l approaches infinity. Such unusual behaviors may be interpreted as a signature for the emergence of an interaction-driven insulating phase [34].

For a random gauge potential, Eqs. (57) and (59) combine to yield

$$\frac{v_\Gamma}{v} = \frac{v_{\Gamma 0}}{v_0}, \tag{64}$$

now C_g can be written as

$$C_g = \frac{v_\Gamma^2 \Delta}{\pi v^2} = \frac{v_{\Gamma 0}^2 \Delta}{\pi v_0^2}, \tag{65}$$

which is a constant. The lines of fixed points are shown in Fig. 6(b). The fixed points are stable in this case. We see from Fig. 7(b) that the fermion velocity either increases or decreases with the decreasing energy scale, depending on the concrete value of α_0, but finally are saturated to certain finite values. This behavior is consistent with previous results obtained in Refs. [34] and [35]. It is argued in Ref. [35] that such disorder dependent fixed point can give rise to a number of interesting properties, such as nonuniversal minimum dc conductivity.

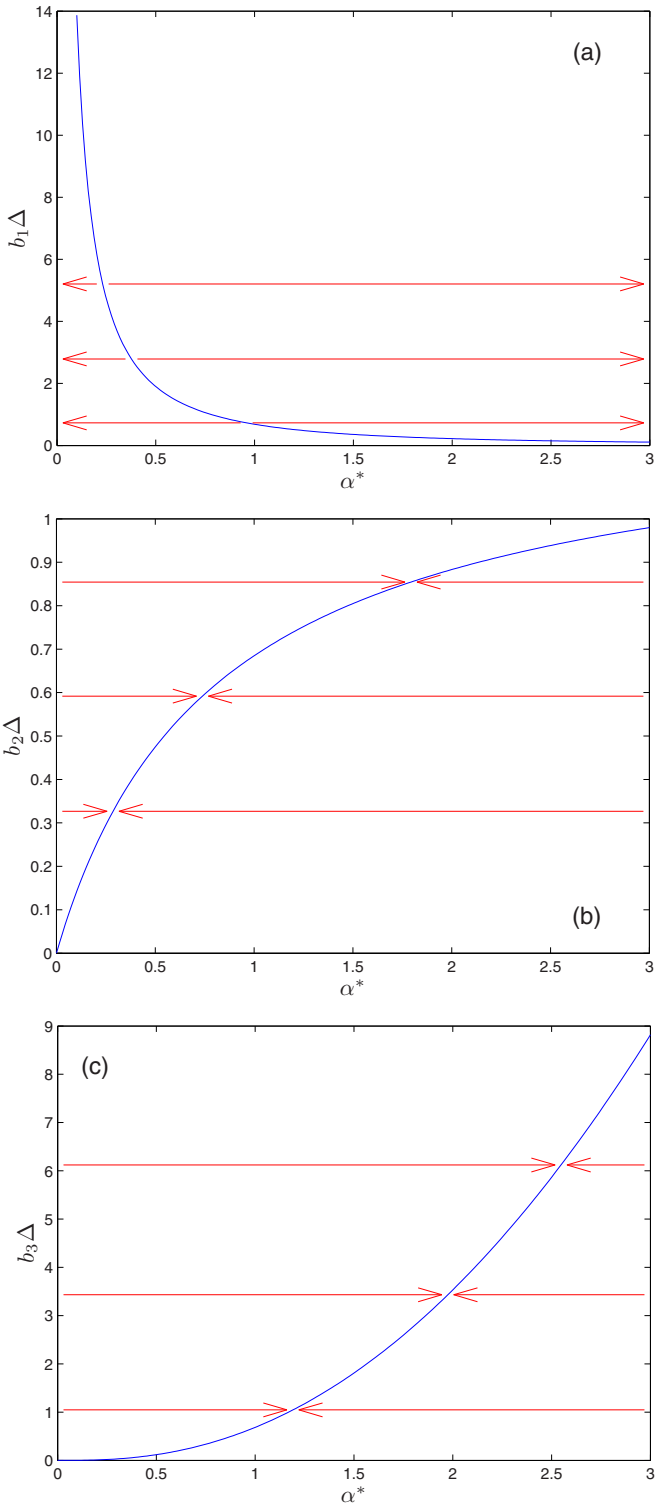

FIG. 6. (Color online) Fixed points for (a) a random chemical potential with $b_1 = \frac{\epsilon^2 v_{\Gamma 0}^2}{e^4}$, (b) a random gauge potential with $b_2 = \frac{v_{\Gamma 0}^2}{v_0^2}$, and (c) random mass with $b_3 = \frac{v_{\Gamma 0}^2 e^4}{\epsilon^2 v_0^4}$.

For random mass, Eqs. (57) and (60) lead to

$$\frac{v_\Gamma}{v^2} = \frac{v_{\Gamma 0}}{v_0^2}, \tag{66}$$

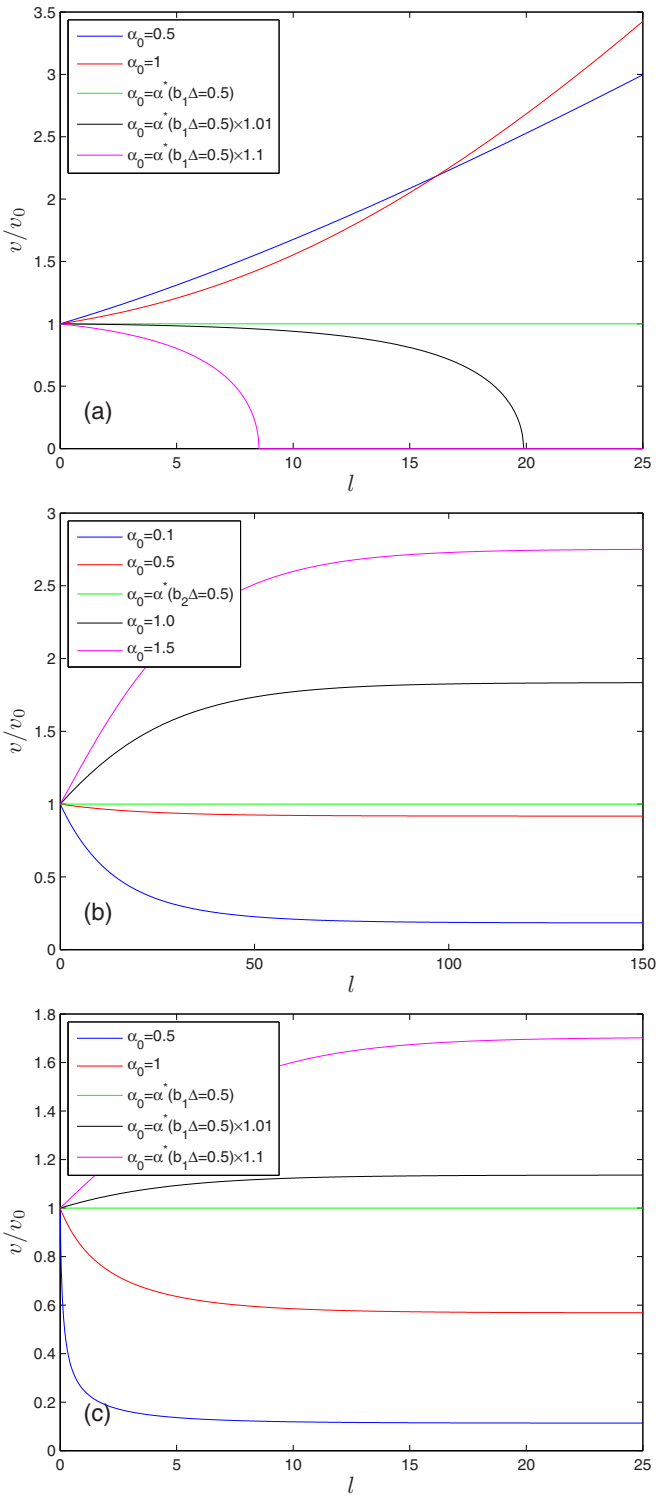

FIG. 7. (Color online) Renormalized fermion velocity for (a) random chemical potential with $b_1\Delta = 0.5$, (b) a random gauge potential with $b_2\Delta = 0.5$, and (c) random mass with $b_3\Delta = 0.5$.

so C_g becomes a function of α,

$$C_g = \frac{v_\Gamma^2 \Delta}{2\pi v^2} = \frac{v_{\Gamma 0}^2 \Delta v^2}{2\pi v_0^4} = \left(\frac{v_{\Gamma 0}^2 \Delta e^4}{2\pi \epsilon^2}\right)\alpha^{-2}. \tag{67}$$

As shown in Fig. 6(c), the fixed points are stable. According to Fig. 7(c), the fermion velocity is also saturated to finite values at the low-energy limit, similar to the case of a random gauge potential. An apparent conclusion is that a random chemical potential leads to very different behaviors compared with a random gauge potential and random mass.

It is necessary to remark on the insulating behavior happening in the presence of a random chemical potential. This presumed insulating state is formed by the interplay of strong Coulomb interaction and a random chemical potential, and is signalled by the absence of a stable fixed point and the divergence of interaction strength. At this stage, it is premature to judge whether this insulator is associated with an excitonic pairing instability [37–48] or a disorder-driven localizationlike state. We feel that the present RG scheme alone is unable to uncover the fundamental nature and detailed properties of such an insulating state. Further research effort is called for to investigate this problem.

D. Disordered and anisotropic case

We finally come to the general and most interesting case in which both anisotropy and disorder are present. We will show that Coulomb interaction and fermion-disorder coupling can result in rich behaviors. The physical properties are very complicated and determined by several parameters, including Coulomb coupling α_{10} and bare velocity ratio $\delta_{10} = v_{20}/v_{10}$. To simplify our analysis, we fix the coupling at $\alpha_{10} = 1$ and examine how the two velocities and their ratio flow as δ_0 is varying.

For a random chemical potential, we remember that v_Γ remains a constant, i.e., $v_\Gamma = v_{\Gamma 0}$. At a fixed Coulomb coupling $\alpha_{10} = 1$, the renormalized velocities $v_{1,2}$ and the ratio v_2/v_1 for different bare values of ratio δ_0 are presented in Fig. 8. In the current case, there is a critical value δ_{0c} lying in the range $0.6 < \delta_{0c} < 0.7$. When $\delta_{0c} < \delta_0 \leqslant 0.9$, the corresponding Coulomb interaction is relatively weak. Both v_1 and v_2 increase monotonically as the energy scale is decreasing, whereas the velocity ratio $v_2/v_1 \to 1$ at the lowest energy, which corresponds to an isotropic fixed point. On the other hand, if $0.5 \leqslant \delta_0 < \delta_{0c}$, the Coulomb interaction becomes sufficiently strong. In this case, both v_1 and v_2 decrease rapidly as the energy is lowering, and are driven to vanish at certain finite energy scale. The latter behavior suggests the disappearance of well-defined quasiparticles, and probably indicate the appearance of an anisotropic insulating phase.

In the presence of a random gauge potential, we know from Eqs. (46), (47), (50), and (51) that

$$\frac{v_{\Gamma 1}}{v_1} = \frac{v_{\Gamma 10}}{v_{10}} \quad \text{and} \quad \frac{v_{\Gamma 2}}{v_2} = \frac{v_{\Gamma 20}}{v_{20}}. \tag{68}$$

The RG flows of velocities $v_{1,2}$ and ratio v_2/v_1 are presented in Fig. 9. It is easy to observe that, both v_1 and v_2 increase initially but finally approach certain finite values. In addition, the ratio v_2/v_1 eventually flows to an isotropic limit, i.e., $v_2/v_1 \to 1$, at the lowest energy. Comparing to the clean and anisotropic case, v_2/v_1 flows to unity more rapidly.

For random mass, the flows of v_1, v_2, v_2/v_1 and v_Γ are depicted in Fig. 10. $v_{1,2}$ and v_Γ are all saturated to finite values

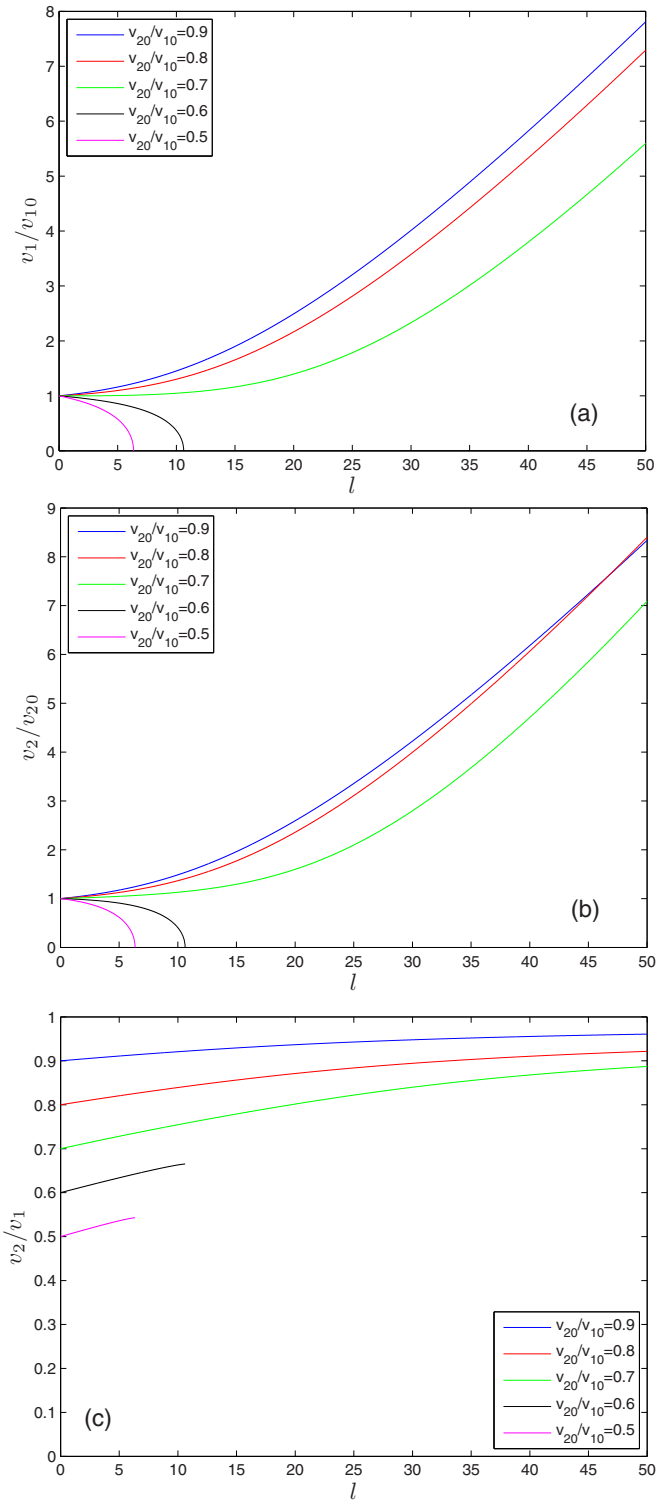

FIG. 8. (Color online) Renormalized v_1, v_2, and v_2/v_1 at fixed coupling $\alpha_{10} = 1$ in the presence of a random chemical potential with $v_{\Gamma 0}^2 \Delta / v_{10}^2 = 0.05$.

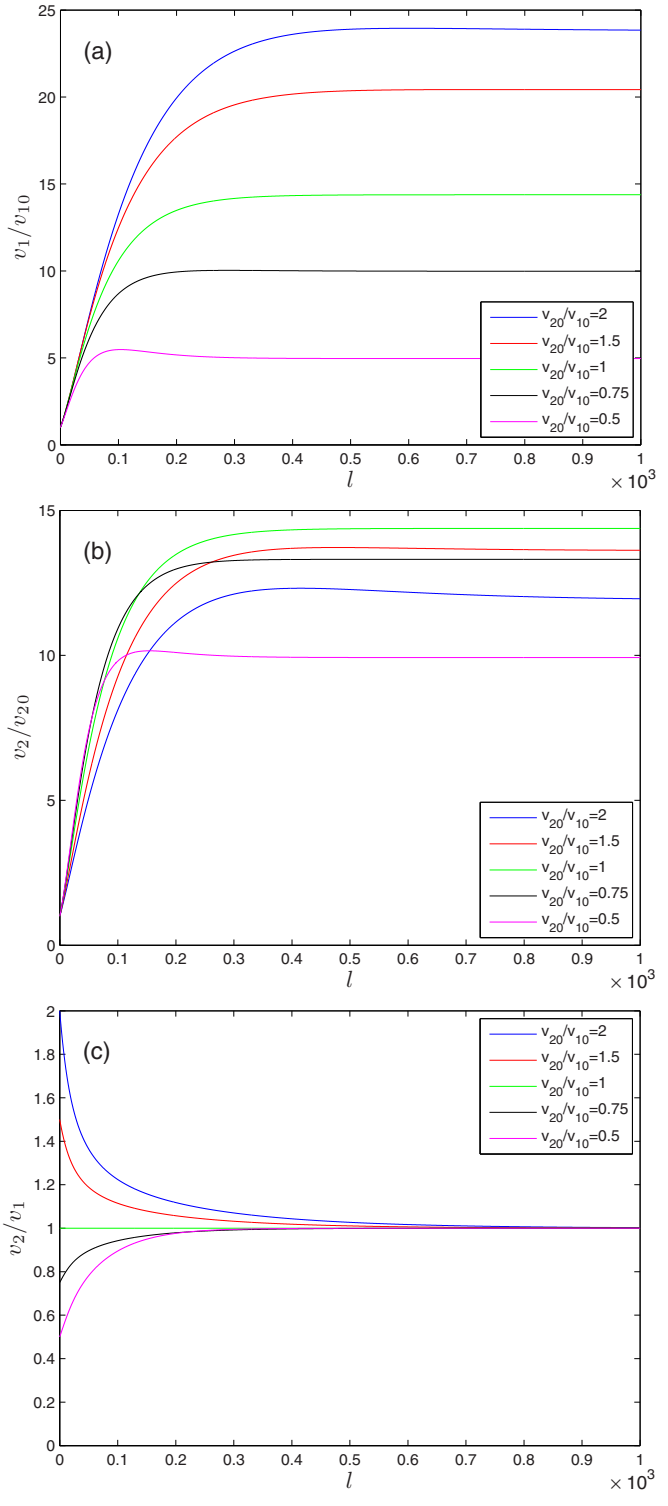

FIG. 9. (Color online) Renormalized v_1, v_2, and v_2/v_1 at fixed coupling $\alpha_{10} = 1$ in the presence of a random gauge potential with $v_{\Gamma 0}^2 \Delta / v_{10}^2 = 0.05$. Here, we take $v_{\Gamma 10} = v_{\Gamma 20} = v_{\Gamma 0}$.

and $v_2/v_1 \to 1$ in the lowest energy limit. These properties are qualitatively very similar to those in the case of a random gauge potential, but is apparently distinct from those in the case of a random chemical potential.

V. INFLUENCE OF FERMION VELOCITY RENORMALIZATION

In the last section, we have already shown that the long-range Coulomb interaction, sometimes in collaboration with disorders, can have remarkable effects on the low-energy

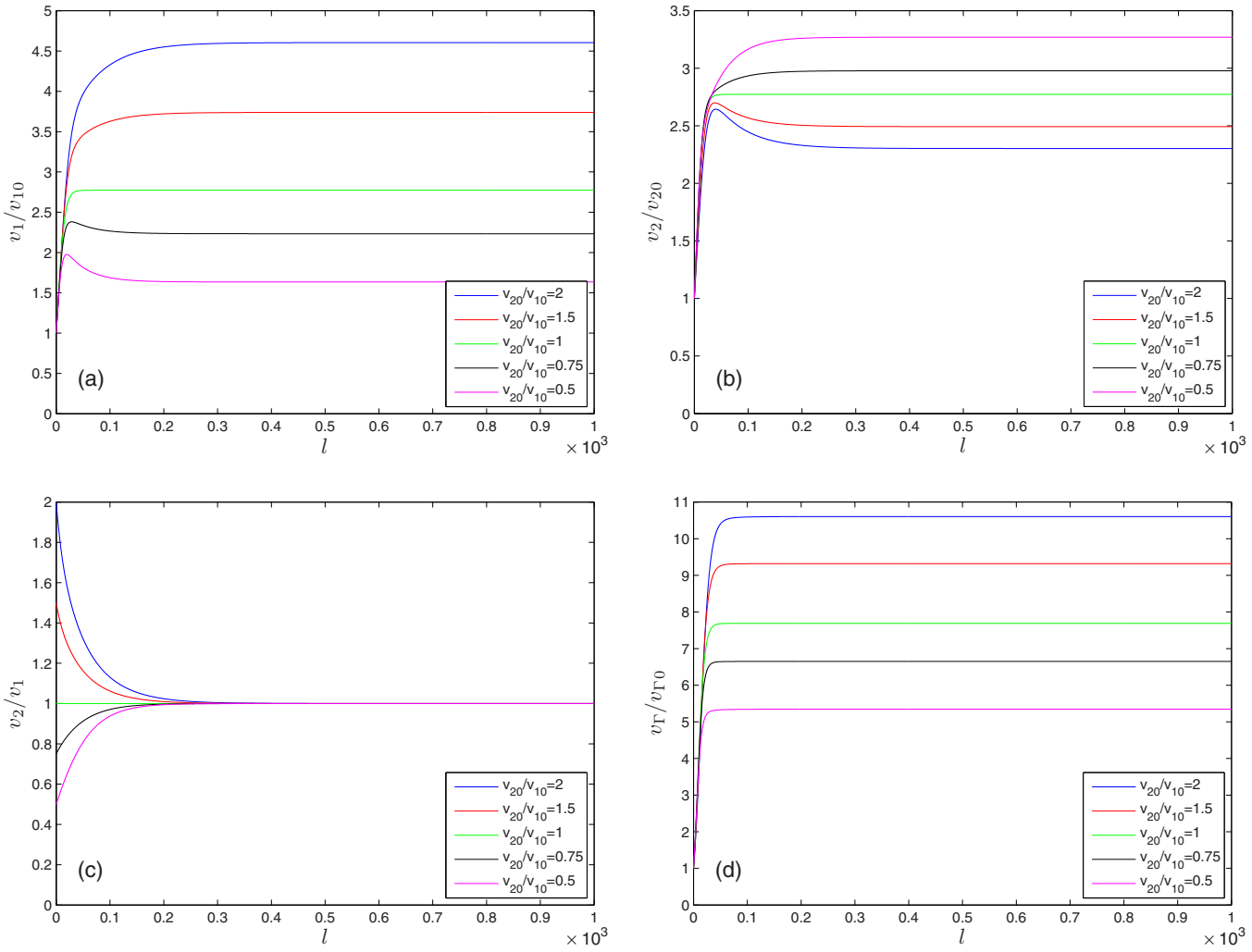

FIG. 10. (Color online) Renormalized v_1, v_2, and v_2/v_1 with $\alpha_{10} = 1$, where $\alpha_{10} = e^2/\epsilon v_{10}$ if there is random mass with $v_{\Gamma 0}^2 \Delta / v_{10}^2 = 0.05$.

properties of fermion velocities and velocity ratio. These effects should manifest themselves in various physical quantities. In order to make these effects more transparent, here we calculate several physical quantities, including quasiparticle damping rate, DOS, and specific heat, and discuss the physical implications of the results.

A. Landau damping rate

Landau damping rate is an important quantity that is frequently used to characterize the effects of inter-particle interactions and to judge whether an interacting many-body system is a Fermi liquid or not. This quantity is intimately related to the wave renormalization function, which can be calculated as follows:

$$Z_f(\omega) = \frac{1}{\left|1 - \frac{\partial}{\partial \omega} \mathrm{Re}\Sigma^R(\omega)\right|}, \tag{69}$$

where $\mathrm{Re}\Sigma^R(\omega)$ is the real part of the retarded fermion self-energy function. However, taking advantage of the RG scheme used in this paper, it is more convenient to write it in the following form:

$$Z_f = e^{\int_0^l (C_0 - C_g) dl}. \tag{70}$$

Using the results obtained in Sec. III, it is easy to get

$$\frac{dZ_f}{dl} = (C_0 - C_g) Z_f, \tag{71}$$

where C_0 and C_g, given in Sec. III A, represent effects of Coulomb interaction and disorders, respectively.

In the clean limit, $C_g = 0$, we have

$$\frac{dZ_f}{dl} = C_0 Z_f. \tag{72}$$

As shown in Fig. 11, Z_f initially decreases with growing l, but is saturated to a finite value as $l \to \infty$, independent of the values of bare velocity ratio. The finiteness of Z_f indicates that the Dirac quasiparticles are well-defined. These results are well consistent with previous RG analysis presented in Ref. [50].

In the presence of disorders, the initial value of C_g becomes finite. We show the flowing behaviors of Z_f with growing l in the presence of a random chemical potential in Fig. 12. At fixed coupling $\alpha_{10} = 1$, there is a critical value δ_{0c} in the range $0.6 < \delta_0 < 0.7$. In the range $\delta_{0c} < \delta_0 \leqslant 0.9$ where the Coulomb interaction is relatively weak, Z_f approaches certain finite value as $l \to \infty$ and the system is a stable Fermi liquid. In

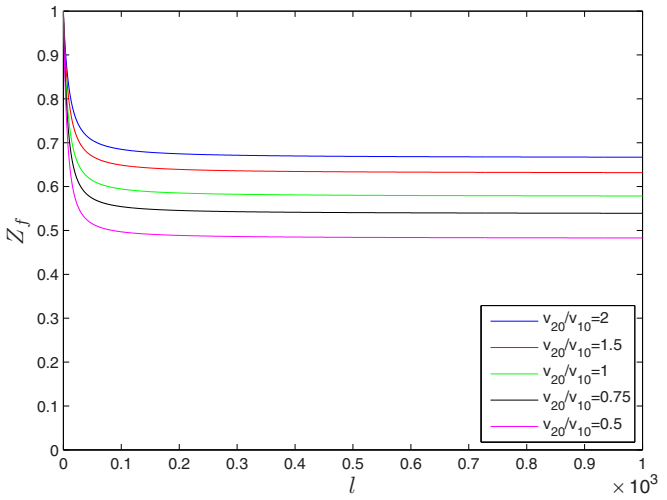

FIG. 11. (Color online) Wave renormalization factor for different v_{20}/v_{10} at fixed coupling $\alpha_{10} = 1$ in the absence of disorders.

such a case, the fermion velocities and Z_f all flow in the same way as that in the clean limit, so the observable quantities (such as DOS and specific heat) are also very similar to those in clean graphene. However, in the range $0.5 < \delta_0 \leqslant \delta_{0c}$ where the Coulomb interaction becomes sufficiently strong, Z_f vanishes even when l is still finite. In addition, the fermion velocities decrease rapidly to zero at certain finite energy scale. These unusual behaviors indicate the instability of Fermi liquid and may, as aforementioned, correspond to the formation of an insulating state, where observable quantities (including DOS and specific heat) should all vanish in the low-energy regime.

The l dependence of Z_f in the presence of a random gauge potential and random mass are shown in Figs. 13 and 14, respectively. The most noticeable common feature of these figures is that Z_f vanishes as $l \to \infty$, which is independent of the concrete values of bare velocity ratio δ_0. This property is a signature of the emergence of non-Fermi liquid behaviors.

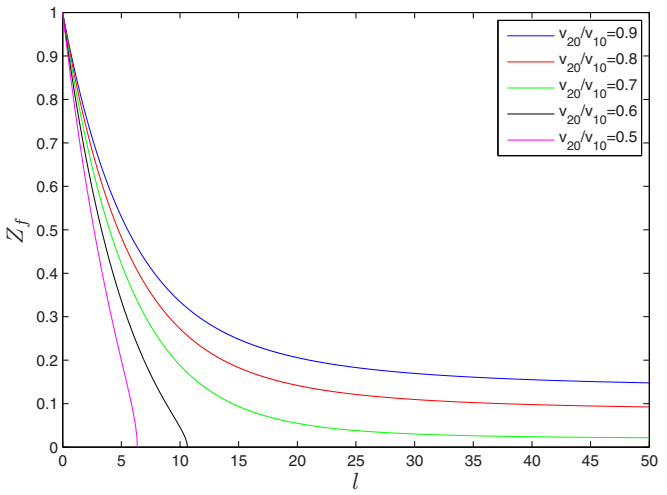

FIG. 12. (Color online) Wave renormalization factor for different v_{20}/v_{10} at fixed coupling $\alpha_{10} = 1$ in the presence of a random chemical potential with $v_{\Gamma 0}^2 \Delta / v_{10}^2 = 0.5$.

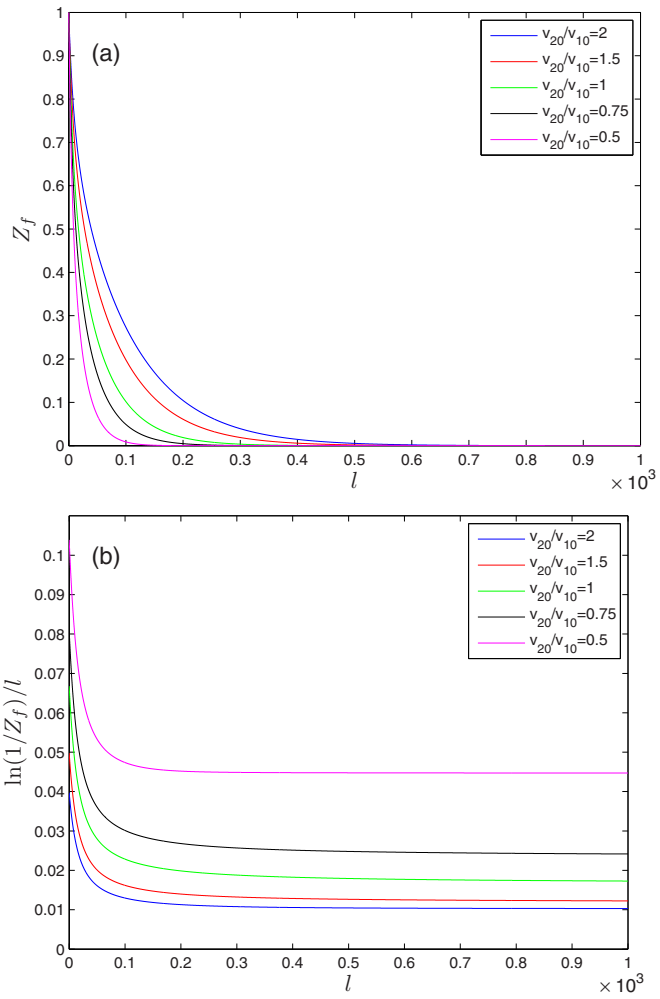

FIG. 13. (Color online) Wave renormalization factor for different v_{20}/v_{10} at fixed coupling $\alpha_{10} = 1$ in the presence of a random gauge potential with $v_{\Gamma 0}^2 \Delta / v_{10}^2 = 0.05$.

More concretely, Z_f behaves as

$$\lim_{l \to \infty} \ln(1/Z_f)/l = \eta \quad (0 < \eta < 1) \tag{73}$$

in the low-energy limit. Here, the magnitude of constant η is determined by the parameters α_{10}, v_{20}/v_{10} and $v_{\Gamma 0}^2 \Delta / v_{10}^2$. We can further write

$$Z_f \propto (e^{-l})^{\eta}. \tag{74}$$

Rewriting the energy as $\omega = \omega_0 e^{-l}$, it is then easy to obtain the real part of retarded self-energy:

$$\mathrm{Re}\Sigma^R(\omega) \propto \omega^{1-\eta}. \tag{75}$$

Using the Kramers-Kronig relation, we obtain the imaginary part of retarded self-energy

$$\mathrm{Im}\Sigma^R(\omega) \propto \omega^{1-\eta}, \tag{76}$$

which is typical non-Fermi liquid behavior since $0 < \eta < 1$. Therefore both a random gauge potential and random mass can lead to breakdown of Fermi liquid and emergence of non-Fermi liquid ground state.

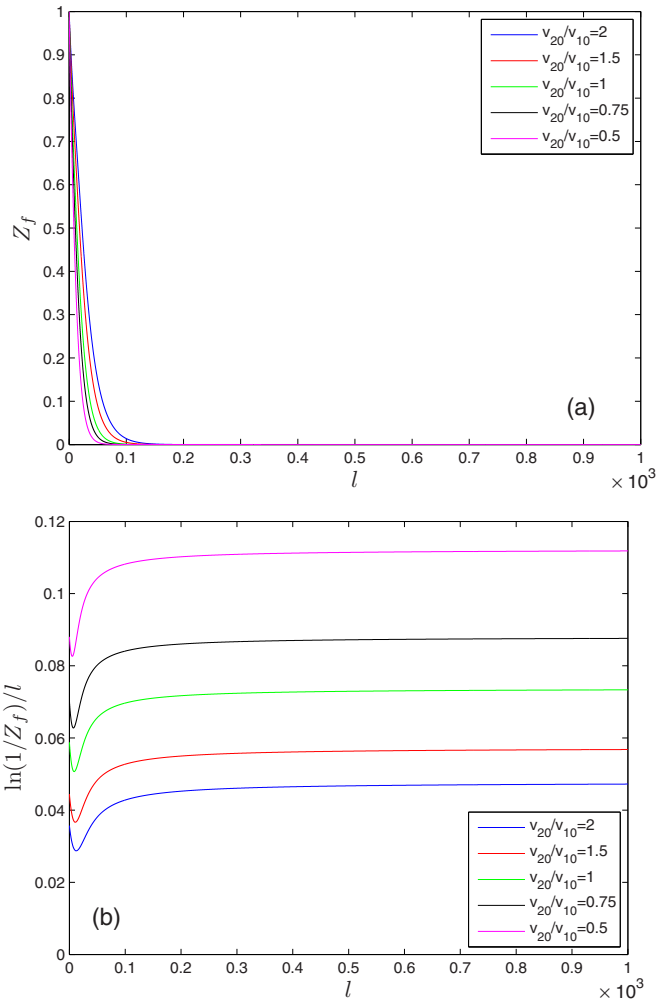

FIG. 14. (Color online) Wave renormalization factor for different v_{20}/v_{10} at fixed coupling $\alpha_{10} = 1$ in the presence of random mass with $v_{\Gamma 0}^2 \Delta / v_{10}^2 = 0.05$.

We have seen in this subsection that the interplay of Coulomb interaction and fermion-disorder interaction can lead to a series of interesting behaviors in graphene samples with an anisotropic Dirac cone. The system may be a normal Fermi liquid, a non-Fermi liquid, or an exotic insulator, depending on the concrete values of bare velocity ratio and the sorts of disorders. In particular, a random chemical potential behaves quite differently from a random gauge potential and random mass.

B. Density of states

We now study the influence of Coulomb interaction on DOS using the method employed by Xu *et al.* [25]. The DOS $\rho(\omega)$ is defined as

$$\rho(\omega) = N \int \frac{dk_1 dk_2}{(2\pi)^2} \mathrm{Tr}\{\mathrm{Im}[G^R(\omega, v_1 k_1, v_2 k_2)]\} = \frac{N}{v_1 v_2} \int \frac{dk_1' dk_2'}{(2\pi)^2} \mathrm{Tr}\{\mathrm{Im}[G^R(\omega, k_1', k_2')]\}, \quad (77)$$

where $G^R(\omega, k_1, k_2)$ is the retarded two-point Green's function (propagator) of Dirac fermions. In the absence of Coulomb interaction, $G^R(\omega, k_1, k_2)$ is simply the retarded free fermion propagator, and it is well-known that DOS exhibits a linear energy dependence, i.e., $\rho(\omega) \propto \omega$. This behavior can be significantly affected by Coulomb interaction and a random gauge potential (random mass). In the present problem, the interaction effects are manifested in the RG flows of $v_{1,2}$ and the anomalous dimension of fermion propagator. After straightforward calculations shown in Appendix D, we find that

$$\frac{d \ln \rho}{d \ln \omega} = \frac{1 + 3C_0 - C_1 - C_2 - 3C_g}{1 - C_0 + C_1 + C_g} \quad (78)$$

for $v_1 > v_2$, and that

$$\frac{d \ln \rho}{d \ln \omega} = \frac{1 + 3C_0 - C_1 - C_2 - 3C_g}{1 - C_0 + C_2 + C_g} \quad (79)$$

for $v_2 > v_1$.

In the clean limit with $C_g = 0$, the ω-dependence of $\rho(\omega)$ for different bare ratios are presented in Fig. 15(a). In the low-energy regime, $\omega \to 0$, we have

$$\frac{\rho(\omega)}{\omega} \sim \frac{1}{\ln(\omega)}. \quad (80)$$

When there is a random gauge potential or random mass, the corresponding $\rho(\omega)$ for different bare ratios are shown in Figs. 15(b) and 15(c). It can be found that $\rho(\omega)$ behaves as

$$\rho(\omega) \sim \omega^{1-\eta} \quad (0 < \eta < 1) \quad (81)$$

in the limit $\omega \to 0$. Comparing this expression to the linear ω dependence of DOS obtained in the noninteracting case, we know that η reflects the corrections arising from Coulomb interaction and disorder scattering.

The dynamical exponent describes how the energy should be rescaled relative to the momenta [74–76]. In our notations, z is encoded in velocities of the Dirac fermions. For a free anisotropic Dirac fermion system, the fermion velocities are constants, so the dynamical exponent $z = 1$. Including the interaction effects, we have two dynamic exponents defined as

$$z_1 = 1 - \frac{d \ln v_1(l)}{dl}, \quad (82)$$

$$z_2 = 1 - \frac{d \ln v_2(l)}{dl}. \quad (83)$$

Due to interplay of Coulomb interaction and a random gauge field (random mass), $v_1(l)/v_2(l) \to 1$ in the lowest energy limit $l \to \infty$, which corresponds to an isotropic fixed point. At the same time, $v_1(l)$ and $v_2(l)$ approach a finite constant. Therefore z satisfies

$$z = z_{1,2}(l \to \infty) = 1. \quad (84)$$

Our result of $\rho(\omega)$ is different from that obtained in Ref. [35], where it is shown that the fermion velocity is saturated to a finite value in the presence of a random gauge

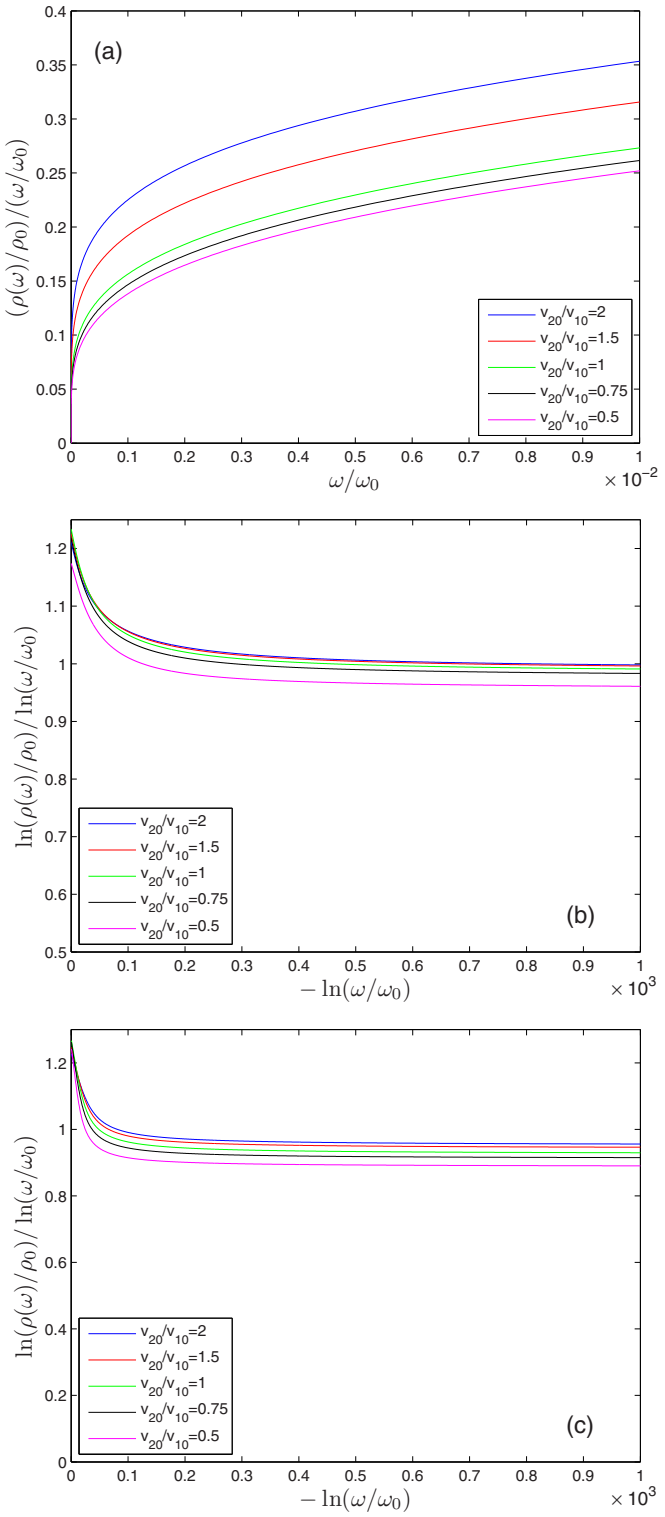

FIG. 15. (Color online) DOS for different v_{20}/v_{10} at fixed coupling $\alpha_{10} = 1$ (a) in the absence of disorders and (b) in the presence of a random gauge potential with $v_{\Gamma 0}^2 \Delta / v_{10}^2 = 0.05$. (c) Wave renormalization factor for different v_{20}/v_{10} at fixed coupling $\alpha_{10} = 1$ in the presence of random mass with $v_{\Gamma 0}^2 \Delta / v_{10}^2 = 0.05$.

potential and that $\rho(\omega) \sim \omega$ since $z = 1$ in the low-energy regime. However, we notice that the nontrivial corrections to DOS actually come from both the change of dynamic exponent and the nontrivial wave function renormalization. Although the dynamical exponent $z = 1$, the wave renormalization function receives a nontrivial correction given in Eq. (74) and lead to non-Fermi liquid like damping rate of Dirac fermions. Consequently, the behaviors of low-energy DOS are disorder dependent, as can be seen from Eq. (81).

C. Specific heat

To calculate specific heat, we also follow the method used in Ref. [25]. The free energy $\mathcal{F} = T \ln \mathcal{Z}/V$ contains the following singular part:

$$\mathcal{F} = (\xi_\tau \xi_x \xi_y)^{-1}, \tag{85}$$

where $\xi_\tau \sim 1/T$, $\xi_x \sim v_1 \xi_\tau$, and $\xi_y \sim v_2 \xi_\tau$. In an interacting anisotropic graphene, the free energy is found to depend on T as

$$\mathcal{F} \sim \frac{1}{v_1 v_2} T^3. \tag{86}$$

The corresponding specific heat is given by

$$C_V = -T \frac{\partial^2 \mathcal{F}}{\partial T^2} \sim \frac{1}{v_1 v_2} T^2. \tag{87}$$

Here, the interaction effects are reflected in the nontrivial flows of v_1 and v_2. After performing calculations shown in Appendix D, we find that C_V varies with T as

$$\frac{d \ln C_V}{d \ln T} \sim 2 + \frac{2C_0 - C_1 - C_2 - 2C_g}{1 - C_0 + C_1 + C_g} \tag{88}$$

for $v_1 > v_2$, and

$$\frac{d \ln C_V}{d \ln T} \sim 2 + \frac{2C_0 - C_1 - C_2 - 2C_g}{1 - C_0 + C_2 + C_g} \tag{89}$$

for $v_2 > v_1$.

In clean graphene, the specific heat $C_V(T)$ for different parameters is shown in Fig. 16(a). We can see that $C_V(T)/T^2 \to 0$ in the limit of $\omega \to 0$. More concretely, we find that

$$\frac{C_V(T)}{T^2} \sim \frac{1}{\ln(T)}, \tag{90}$$

which is consistent with the results obtained in Ref. [52].

In the presence of a random gauge potential or random mass, the corresponding specific heat $C_V(T)$ for different parameters are shown in Figs. 16(b) and 16(c). $C_V(T)$ behaves as

$$C_V(T) \sim T^2 \tag{91}$$

in the limit $T \to 0$. General scaling analysis shows that the specific heat should satisfy $C_V(T) \propto T^{d/z}$ [75,77], where d is the spatial dimension and z is the dynamical exponent. In the present case, the fermion velocities are saturated to finite values and the dynamical exponent $z \to 1$ in the low-energy regime, so $C_V(T) \propto T^2$. It might seem strange that, the DOS is not linear in ω as shown in Eq. (81) but the specific heat still exhibits quadratic T-dependence. This can be understood as follows. When the Dirac fermion propagator acquires a

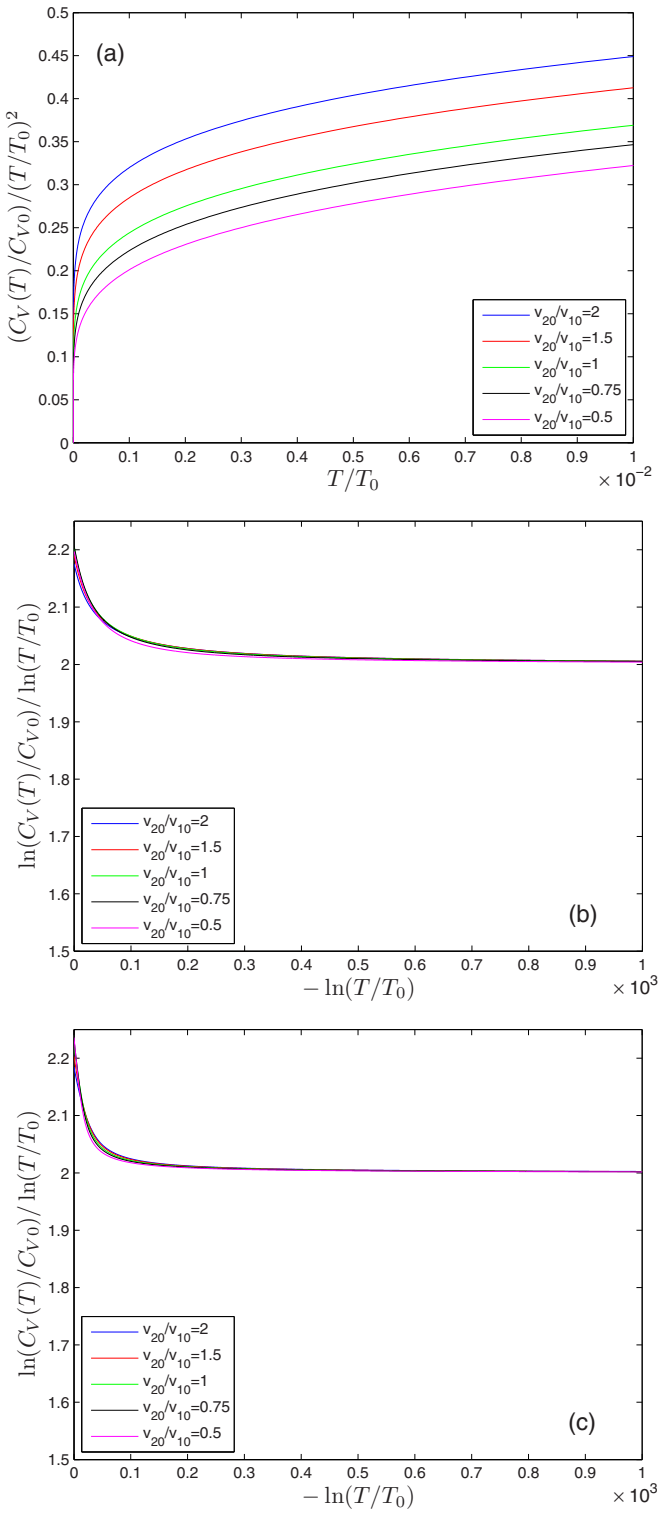

FIG. 16. (Color online) Specific heat for different v_{20}/v_{10} at fixed coupling $\alpha_{10} = 1$ (a) in the absence of disorders, and (b) in the presence of a random gauge potential with $v_{\Gamma 0}^2 \Delta / v_{10}^2 = 0.05$. (c) Specific heat for different v_{20}/v_{10} at fixed coupling $\alpha_{10} = 1$ in the presence of a random mass with $v_{\Gamma 0}^2 \Delta / v_{10}^2 = 0.05$.

finite positive anomalous dimension η, the Landau damping rate of the fermion takes non-Fermi liquid behavior and the DOS is no longer linear in energy. However, the anomalous dimension does not change the T-dependence of specific heat. To better understand this problem, we make a brief discussion in Appendix E.

VI. DYNAMICAL GAP GENERATION IN ANISOTROPIC GRAPHENE

Recently, a number of theoretical and numerical works [37–48] have predicted that the long-range Coulomb interaction between massless Dirac fermions in graphene may generate a dynamical gap by forming excitonic pairs and consequently lead to semimetal-insulator transition. This gap-generating mechanism is of great interest to theorists because it can be considered as a concrete condensed-matter realization of the nonperturbative phenomenon of dynamical chiral symmetry breaking, which was first proposed by Nambu and Jona-Lasinio [78] and has played a significant role in the development of modern particle physics [79,80]. From a technological point of view, a gapped graphene is more promising than a gapless one as a candidate for manipulating novel electronic devices [45,81]. For these reasons, the mechanism of dynamical gap generation and the resultant semimetal-insulator transition have stimulated considerable effort in recent years.

Earlier calculations carried out using the DS equation approach have reached an optimistic conclusion that a dynamical gap is generated by Coulomb interaction in suspended clean graphene [37–42]. However, a number of approximations are adopted in these works, which more or less lowers the reliability of this conclusion (see Ref. [48] for a brief review of these approximations). More recently, we have revisited this problem by improving most of these approximations and found that the Coulomb interaction in suspended graphene is indeed not strong enough to open a dynamical gap [48]. At the same time, experimentalists have measured the energy spectrum of suspended graphene at ultralow temperatures and observed no evidence of insulating behavior [63,82]. A key factor that weakens the effective Coulomb interaction is the unusual renormalization of fermion velocity. It is known that the Coulomb interaction coupling $\alpha \propto e^2/v$ with v being the universal fermion velocity in isotropic graphene. As v diverges at the lowest energy, α tends to vanish, which means the effective interaction strength is significantly reduced. Apparently, fermion velocity renormalization plays a crucial role in this problem, and needs to be carefully treated.

As shown in the last sections, the renormalization of fermion velocities in anisotropic graphene can be different from that in the case of isotropic graphene. Such an important difference may lead to remarkable change of the effective strength of Coulomb interaction. It is therefore very interesting to investigate how dynamical gap generation is affected by the velocity anisotropy. In this section, we are particularly interested in whether the velocity anisotropy enhances or suppresses dynamical gap generation in clean graphene. The nonperturbative DS equation approach [37–42,46,47,78–80,83] will be used to address this issue since the conventional perturbative expansion is unable to tackle the nonperturbative phenomenon of dynamical gap generation. Moreover, in this section, we will not consider

FIG. 17. Diagrams for the fermion self-energy in the DS equation approach. The thick solid line denotes a dressed fermion propagator.

the effects of disorders, which are technically difficult to be incorporated in the self-consistent DS equation [40,47].

After including the interaction induced self-energy corrections, the free fermion propagator, given in Eq. (5), will be renormalized to the following full propagator:

$$G(i\omega,\mathbf{k}) = \frac{1}{-i\omega A_0\gamma_0 + v_1k_1A_1\gamma_1 + v_2k_2A_2\gamma_2 + m}, \quad (92)$$

where m represents a finite dynamical gap and $A_{0,1,2}$ are the three components of wave function renormalization. According to the Feynman diagram shown in Fig. 17, the dressed fermion propagator is related to the free one via the following DS equation:

$$G^{-1}(i\varepsilon,\mathbf{p}) = G_0^{-1}(i\varepsilon,\mathbf{p}) + \int \frac{d\omega}{2\pi}\frac{d^2\mathbf{k}}{(2\pi)^2}\gamma_0 G(i\omega,\mathbf{k})\gamma_0 \times D(i(\varepsilon-\omega),\mathbf{p}-\mathbf{k}). \quad (93)$$

To the lowest order of $1/N$ expansion, we take $A_0 = A_1 = A_2 = 1$ for simplicity and substitute Eq. (92) into Eq. (93). After straightforward calculations, we obtain an integral equation for the dynamical gap m,

$$m(i\varepsilon,p_1,p_2) = \int\frac{d\omega}{2\pi}\int\frac{dk_x}{2\pi}\int\frac{dk_y}{2\pi} \times \frac{m(i\omega,k_1,k_2)}{\omega^2+v_1^2k_1^2+v_2^2k_2^2+m^2(i\omega,k_1,k_2)} \times \frac{1}{\frac{|\mathbf{q}|}{\frac{2\pi e^2}{\epsilon}} + \frac{N}{8v_1v_2}\frac{v_1^2q_1^2+v_2^2q_2^2}{\sqrt{\Omega^2+v_1^2q_1^2+v_2^2q_2^2}}}, \quad (94)$$

where $\Omega = \epsilon - \omega$, $q_1 = p_1 - k_1$, and $q_2 = p_2 - k_2$. This nonlinear equation is very complicated and needs to be numerically solved. A finite fermion gap is generated by the Coulomb interaction once this equation develops a nontrivial solution. In the anisotropic case, the equation of m depends on energy and two components of momentum separately, which makes it difficult to solve the integral equation numerically. In order to simplify the numerical computations, we adopt several frequently used approximations, and then compare the results obtained under these approximations. If some common features can be extracted from all the results, then we can qualitatively judge whether spatial anisotropy is in favor of dynamical gap generation or not.

We will consider six different approximations. First, we consider the instantaneous approximation, which drops the energy dependence of polarization function [37–39] as follows:

$$\frac{1}{\frac{|\mathbf{q}|}{\frac{2\pi e^2}{\epsilon}} + \frac{N}{8v_1v_2}\frac{v_1^2q_1^2+v_2^2q_2^2}{\sqrt{\Omega^2+v_1^2q_1^2+v_2^2q_2^2}}} \to \frac{1}{\frac{|\mathbf{q}|}{\frac{2\pi e^2}{\epsilon}} + \frac{N}{8v_1v_2}\sqrt{v_1^2q_1^2+v_2^2q_2^2}}. \quad (95)$$

Now the gap equation is simplified to

$$m(p_1,p_2) = \frac{1}{2}\int\frac{dk_1}{2\pi}\int\frac{dk_2}{2\pi}\frac{m(k_1,k_2)}{\sqrt{k_1^2+\delta^2k_2^2+m^2(k_1,k_2)}} \times \frac{1}{\frac{\sqrt{q_1^2+q_2^2}}{2\pi\alpha_1} + \frac{N}{8\delta}\sqrt{q_1^2+\delta^2q_2^2}}, \quad (96)$$

where $\delta = v_2/v_1$. In the derivation of this gap equation, we have performed the re-scaling transformations

$$v_1p_{1,2} \to p_{1,2}, \quad v_1k_{1,2} \to k_{1,2}. \quad (97)$$

Such transformation will also be used in the calculations to be performed below.

Second, we utilize the following approximation [41]:

$$\frac{1}{\frac{|\mathbf{q}|}{\frac{2\pi e^2}{\epsilon}} + \frac{N}{8v_1v_2}\frac{v_1^2q_1^2+v_2^2q_2^2}{\sqrt{\Omega^2+v_1^2q_1^2+v_2^2q_2^2}}} \to \frac{1}{\frac{|\mathbf{q}|}{\frac{2\pi e^2}{\epsilon}} + \frac{N}{8\sqrt{2}v_1v_2}\sqrt{v_1^2q_1^2+v_2^2q_2^2}}. \quad (98)$$

The corresponding gap equation has the form

$$m(p_1,p_2) = \frac{1}{2}\int\frac{dk_1}{2\pi}\int\frac{dk_2}{2\pi}\frac{m(k_1,k_2)}{\sqrt{k_1^2+\delta^2k_2^2+m^2(k_1,k_2)}} \times \frac{1}{\frac{\sqrt{q_1^2+q_2^2}}{2\pi\alpha_1} + \frac{N}{8\sqrt{2}\delta}\sqrt{q_1^2+\delta^2q_2^2}}. \quad (99)$$

Third, we consider the approximation used in Ref. [42], which assumes that $m(i\epsilon,\mathbf{p})$ is energy-independent, i.e.,

$$m(i\epsilon,p_1,p_2) \to m(p_1,p_2). \quad (100)$$

Applying this approximation leads to

$$m(p_1,p_2) = \alpha_1\int\frac{dk_1}{2\pi}\int\frac{dk_2}{2\pi}\frac{1}{\sqrt{q_1^2+q_2^2}} \times \frac{m(k_1,k_2)J(d,g)}{\sqrt{k_1^2+\delta^2k_2^2+m^2(k_1,k_2)}}, \quad (101)$$

where

$$J(d,g) = \frac{(d^2-1)[\pi - gc(d)] + dg^2c(g)}{d^2+g^2-1}, \quad (102)$$

with

$$c(x) = \begin{cases} \frac{2}{\sqrt{1-x^2}}\cos^{-1}(x) & x<1 \\ \frac{2}{\sqrt{x^2-1}}\cosh^{-1}(x) & x>1 \\ 2 & x=1 \end{cases}, \quad (103)$$

$$d = \sqrt{\frac{k_1^2+\delta^2k_2^2+m^2(k_1,k_2)}{q_1^2+\delta^2q_2^2}}, \quad (104)$$

$$g = \frac{N\pi\alpha_1\sqrt{q_1^2+\delta^2q_2^2}}{4\delta\sqrt{q_1^2+q_2^2}}. \quad (105)$$

In these approximations, the fermion velocities v_1 and v_2 are assumed to take bare values. However, both v_1 and v_2

are indeed strongly renormalized by the Coulomb interaction. To incorporate the feedback effects of strong velocity renormalization on the DS generation, we can replace the bare fermion velocities by the renormalized, momentum-dependent velocities [41], $v_{1,2} \to v_{1,2}(k)$, which are determined by the solutions of Eqs. (54) and (55), and then solve the new gap equations.

We present the numerical results for the dependence of dynamical gap $m(0)$ on δ and α_1 obtained by applying the first three approximations in (a), (b), and (c) of Fig. 18,

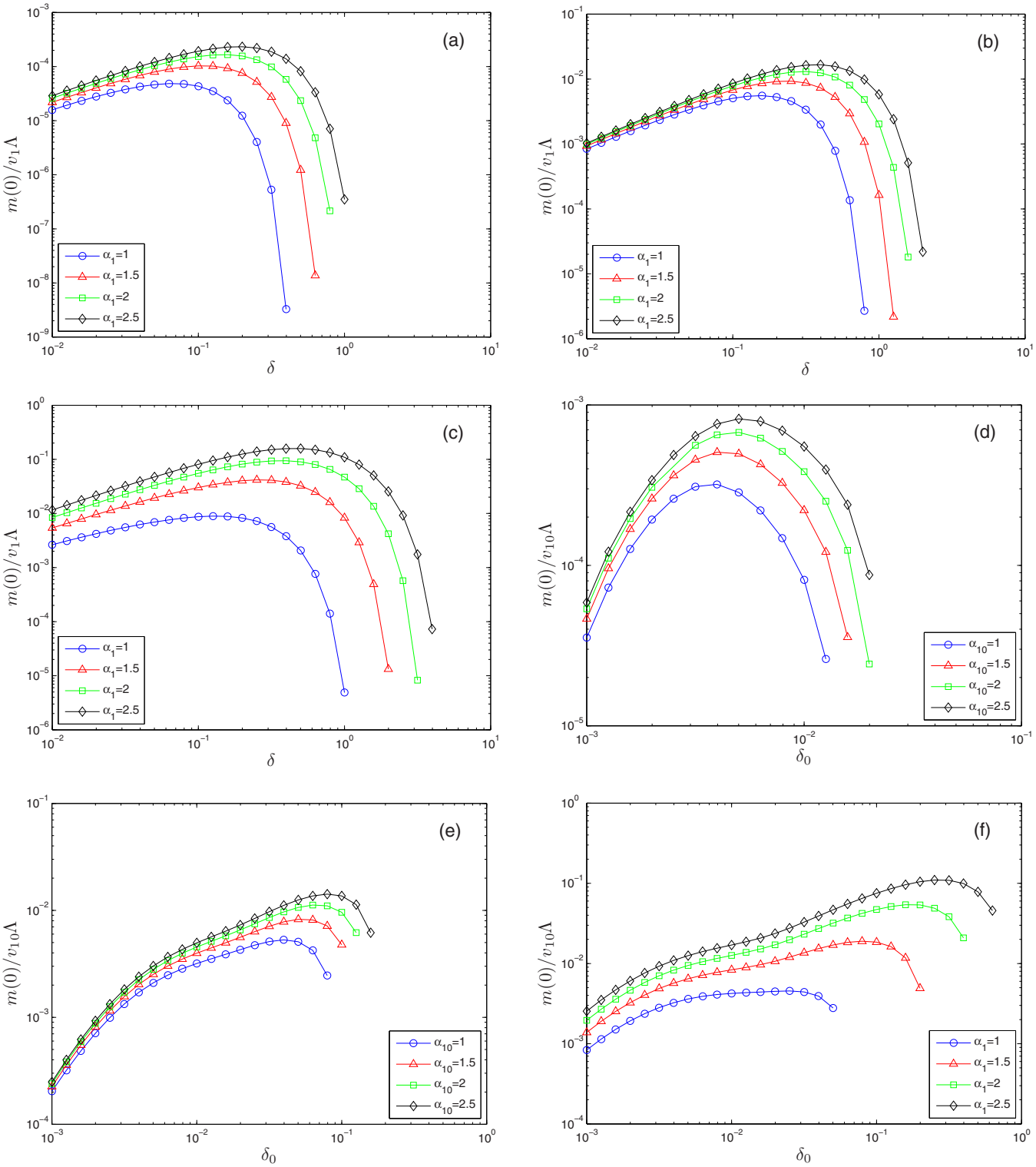

FIG. 18. (Color online) Dependence of the dynamical gap $m(0)$ on the bare velocity ratio δ obtained under a series of approximations: (a) approximation (95); (b) approximation (98); and (c) approximation (100). In (d), (e), and (f), the bare fermion velocities used to obtain the results of (a), (b), and (c) are replaced by the renormalized velocities obtained from the solutions of (54) and (55).

respectively. We then replace the bare velocities appearing in Eqs. (96), (99), and (101) by the corresponding renormalized velocities, and show the results in (d), (e), and (f) of Fig. 18, respectively. From these six figures, we see that the quantitative results of dynamical gap are very sensitive to the concrete approximations and significantly differ from each other.

Strictly speaking, all the results of $m(0)$ presented in Fig. 18 may not correspond to the precise values of the dynamical gap. Nevertheless, one can extract a common feature from the results obtained in all these six cases: at some fixed coupling $\alpha_1 = e^2/v_1\epsilon$, the dependence of $m(0)$ on bare velocity ratio δ is not monotonic. As δ is growing from zero, the dynamical gap $m(0)$ first increases, then reaches its maximal value at certain critical ratio δ_c, and finally decreases rapidly. This common feature is independent of the concrete magnitudes of the coupling constant α_1, provided that α_1 is sufficiently large. Certainly, the precise positions of the peaks of $m(0)$ are strongly case dependent.

We first look at the results presented in Figs. 18(a)–18(c). At certain fixed ratio δ, we see that the dynamical gap is always enhanced as the coupling α_1 increases, which in turn drives both v_1 and v_2 to decrease for a given ε. If we fix the value of α_1 and increase the ratio δ, the dynamical gap is initially enhanced but then gets suppressed once δ exceeds some critical value. For fixed α_1, the deceasing of δ from 1 results in two effects: reduction of v_2 and enhancement of velocity anisotropy. The nonmonotonic dependence of the dynamic gap on δ implies that these two effects are competing with each other. Since the first effect always enhances dynamical gap, the second effect should always suppress dynamical gap. At fixed coupling α_1, increasing δ from 1 also leads to two effects: growth of v_2 and enhancement of velocity anisotropy. Both of these two effects are capable of suppressing the dynamical gap. Indeed, Figs. 18(a)–18(c) clearly shows that the dynamical gap is always suppressed as δ increases from $\delta = 1$.

It is also interesting to make a comparison between Figs. 18(a) and 18(d). For smaller values of bare ratio δ_0, the velocity renormalization promotes the happening of dynamical gap generation. However, for relatively larger values of δ_0, the velocity renormalization suppresses the dynamical gap. The same conclusion can be drawn if we compare Fig. 18(b) with Fig. 18(e), and compare Fig. 18(c) with Fig. 18(f).

In conclusion, our calculations have shown that the dynamical gap is enhanced (suppressed) as the fermion velocities decrease (increase), but is always suppressed as the velocity anisotropy increases. Apparently, the velocity anisotropy turns out to be a negative factor for the occurrence of dynamical gap generation.

In this section, we have acquired only the δ-dependence of dynamical gap for several fixed values of coupling α_1. Unfortunately, it is difficult to obtain a quantitatively reliable δ dependence of critical coupling α_{1c} that separates the semimetal and insulating phases, primarily because of the complexity of anisotropic DS equation. However, the unusual δ-dependence of dynamical gap presented in Fig. 18 suggests that it is both interesting and necessary to solve the anisotropic DS equation more precisely. We expect a large scale Monte Carlo simulation [43,44] can be performed to investigate this issue and clarify some crucial problems.

VII. SUMMARY AND DISCUSSIONS

In this paper, we have investigated the influence of long-range Coulomb interaction on various properties of Dirac fermions in the context of graphene with a spatial anisotropy by performing detailed RG calculations based on $1/N$ expansion. We find that the renormalized fermion velocities increase monotonously as the energy scale decreases and the system approaches a stable isotropic fixed point in the low-energy regime.

The effects of three types of static disorders, including a random chemical potential, a random gauge potential, and random mass, are also examined using RG techniques. We have shown that the interplay of Coulomb interaction and fermion-disorder coupling leads to a series of unusual behaviors. In the case of random chemical potential, the anisotropic system approaches an isotropic fixed point for weak Coulomb interaction. However, when the Coulomb interaction is sufficiently strong, the fermion velocities are driven to vanish in finite energy scale and the system is very likely an anisotropic insulator. On the other hand, both random gauge potential and random mass turn the anisotropic system to a stable isotropic fixed point in the low-energy regime, at an efficiency higher than that in the case of clean anisotropic graphene. An apparent conclusion is that random chemical potential leads to very different behaviors compared with random gauge potential and random mass.

In order to understand the unusual behaviors produced by Coulomb interaction and disorders more explicitly, we have calculated several physical quantities, including wave renormalization factor, Landau damping rate, DOS, and specific heat, after taking into account singular renormalization of fermion velocities. These quantities exhibit non-Fermi liquid behaviors in many cases. Once again, the random chemical potential is found to result in qualitatively different behaviors of these quantities compared to the other two disorders.

We have further studied the nonperturbative effects of Coulomb interaction and included the velocity anisotropy into the DS gap equation. We have acquired the dependence of dynamical gap on the coupling α_1 and the velocity ratio δ, at several different approximations of the DS equation. Our results demonstrate that the decreasing (increasing) fermion velocities can enhance (suppress) the dynamic gap. In addition, increasing velocity anisotropy tends to weaken the effective strength of Coulomb interaction and therefore suppressed the dynamical gap.

Recently, with the help of symmetry considerations, Herbut *et al.* have studied semimetal-insulator transition [84,85] and semimetal-superconductor transition [86,87] in honeycomb lattices, and systematically considered the corresponding quantum critical behaviors. It would be interesting to generalize these studies to the case of anisotropic graphene.

ACKNOWLEDGMENTS

We thank Jing Wang for helpful discussions. J.R.W. acknowledges the support by the MPG-CAS doctoral promotion programme. G.Z.L. acknowledges the support by the National Natural Science Foundation of China under Grant Nos. 11074234 and 11274286.

APPENDIX A: FERMION SELF-ENERGY CORRECTION DUE TO COULOMB INTERACTION

In this Appendix, we provide the details for the calculations of fermion self-energy due to Coulomb interaction. The self-energy is given by

$$\Sigma_C(i\omega,\mathbf{k}) = -\int \frac{d^2\mathbf{q}}{(2\pi)^2}\int \frac{d\Omega}{2\pi}\gamma_0 G_0(i(\Omega+\omega),\mathbf{q}+\mathbf{k})\gamma_0 \times V(i\Omega,\mathbf{q}). \tag{A1}$$

An ultraviolet cutoff is introduced by multiplying both fermion propagator and boson propagator by a smooth cutoff function $\mathcal{K}(\mathbf{k}^2/\Lambda^2)$. Here, $\mathcal{K}(y)$ is an arbitrary function with $\mathcal{K}(0)=1$. It falls off rapidly with y at $y\sim 1$, e.g., $\mathcal{K}(y)=e^{-y}$. However, the results will be independent of the particular choices of $\mathcal{K}(y)$. Now the self-energy becomes

$$\Sigma_C(i\omega,\mathbf{k}) = -\int \frac{d^2\mathbf{q}}{(2\pi)^2}\int \frac{d\Omega}{2\pi}\gamma_0 G_0(i(\Omega+\omega),\mathbf{q}+\mathbf{k})\gamma_0 \times V(i\Omega,\mathbf{q})\mathcal{K}\left(\frac{(\mathbf{q}+\mathbf{k})^2}{\Lambda^2}\right)\mathcal{K}\left(\frac{\mathbf{q}^2}{\Lambda^2}\right). \tag{A2}$$

Namely,

$$\Sigma_C(K) = -\int \frac{d^3Q}{(2\pi)^3}F(Q+K)V(Q)\mathcal{K}\left(\frac{(\mathbf{q}+\mathbf{k})^2}{\Lambda^2}\right) \times \mathcal{K}\left(\frac{\mathbf{q}^2}{\Lambda^2}\right), \tag{A3}$$

where

$$F(\Omega+\omega,\mathbf{q}+\mathbf{k}) = \frac{i\,(\Omega+\omega)\,\gamma_0 + v_1(q_1+k_1)\gamma_1 + v_2(q_2+k_2)\gamma_2}{(\Omega+\omega)^2 + v_1^2\,(q_1+k_1)^2 + v_2^2\,(q_2+k_2)^2} \tag{A4}$$

and $K\equiv(\omega,\mathbf{k})$ and $Q\equiv(\Omega,\mathbf{q})$ are 3-momenta. One can make the following expansion to the first order of K_μ:

$$F(Q+K)\mathcal{K}\left(\frac{(\mathbf{q}+\mathbf{k})^2}{\Lambda^2}\right) \approx K_\mu\left[\frac{\partial F(Q)}{\partial Q_\mu}\mathcal{K}\left(\frac{\mathbf{q}^2}{\Lambda^2}\right) + F(Q)\frac{2q_\mu}{\Lambda^2}\mathcal{K}'\left(\frac{\mathbf{q}^2}{\Lambda^2}\right)\right], \tag{A5}$$

where $K_\mu=(\omega,\mathbf{k})$, $k_\mu=(0,\mathbf{k})$. Therefore the self-energy is rewritten as

$$\Sigma_C(K) = -K_\mu\int \frac{d^3Q}{(2\pi)^3}\left[\frac{\partial F(Q)}{\partial Q_\mu}V(Q)\mathcal{K}^2\left(\frac{\mathbf{q}^2}{\Lambda^2}\right) + F(Q)V(Q)\frac{2q_\mu}{\Lambda^2}\mathcal{K}\left(\frac{\mathbf{q}^2}{\Lambda^2}\right)\mathcal{K}'\left(\frac{\mathbf{q}^2}{\Lambda^2}\right)\right], \tag{A6}$$

which yields

$$\frac{d\Sigma_C(K)}{d\ln\Lambda} = K_\mu\int \frac{d^3Q}{(2\pi)^3}\left\{\left[\frac{\partial F(Q)}{\partial Q_\mu}\frac{4\mathbf{q}^2}{\Lambda^2} + F(Q)\frac{4q_\mu}{\Lambda^2}\right] \times V(Q)\mathcal{K}\left(\frac{\mathbf{q}^2}{\Lambda^2}\right)\mathcal{K}'\left(\frac{\mathbf{q}^2}{\Lambda^2}\right) + F(Q)V(Q)\frac{4\mathbf{q}^2q_\mu}{\Lambda^4}\left[\mathcal{K}'^2\left(\frac{\mathbf{q}^2}{\Lambda^2}\right) + \mathcal{K}\left(\frac{\mathbf{q}^2}{\Lambda^2}\right)\mathcal{K}''\left(\frac{\mathbf{q}^2}{\Lambda^2}\right)\right]\right\}. \tag{A7}$$

Converting to cylindrical coordinates by defining

$$Q_\mu = y\Lambda(v_1x,\cos\theta,\sin\theta), \tag{A8}$$

$$\hat{Q}_\mu = (v_1x,\cos\theta,\sin\theta), \tag{A9}$$

$$q_\mu = y\Lambda(0,\cos\theta,\sin\theta), \tag{A10}$$

$$\hat{q}_\mu = (0,\cos\theta,\sin\theta), \tag{A11}$$

$$d^3Q = y^2\Lambda^3v_1dxdyd\theta, \tag{A12}$$

we have

$$\frac{d\Sigma_C(K)}{d\ln\Lambda} = K_\mu\frac{v_1}{2\pi^3}\int_{-\infty}^{+\infty}dx\int_0^{2\pi}d\theta\left\{\left[\frac{\partial F(\hat{Q})}{\partial\hat{Q}_\mu} + F(\hat{Q})\hat{q}_\mu\right] \times V(\hat{Q})\int_0^{+\infty}dyy\mathcal{K}(y^2)\mathcal{K}'(y^2) + F(\hat{Q})V(\hat{Q})\hat{q}_\mu \times \int_0^{+\infty}dyy^3[\mathcal{K}'^2(y^2) + \mathcal{K}(y^2)\mathcal{K}''(y^2)]\right\}. \tag{A13}$$

Since

$$\int_0^{+\infty}dyy\mathcal{K}(y^2)\mathcal{K}'(y^2) = -\frac{1}{4}, \tag{A14}$$

$$\int_0^{+\infty}dyy^3[\mathcal{K}'^2(y^2) + \mathcal{K}(y^2)\mathcal{K}''(y^2)] = \frac{1}{4}, \tag{A15}$$

one can further obtain

$$\frac{d\Sigma_C(K)}{d\ln\Lambda} = -\frac{v_1K_\mu}{8\pi^3}\int_{-\infty}^{+\infty}dx\int_0^{2\pi}d\theta\frac{\partial F(\hat{Q})}{\partial\hat{Q}_\mu}V(\hat{Q}), \tag{A16}$$

where

$$F(\hat{Q}) = \frac{1}{v_1}\frac{ix\gamma_0 + \cos\theta\gamma_1 + (v_2/v_1)\sin\theta\gamma_2}{x^2+\cos^2\theta+(v_2/v_1)^2\sin^2\theta}, \tag{A17}$$

$$V(\hat{Q}) = v_1\mathcal{G}(x,\theta), \tag{A18}$$

with

$$\mathcal{G}^{-1}(x,\theta) = \frac{1}{\frac{2\pi e^2}{\epsilon v_1}} + \frac{N}{8(v_2/v_1)} \times \frac{\cos^2\theta+(v_2/v_1)^2\sin^2\theta}{\sqrt{x^2+\cos^2\theta+(v_2/v_1)^2\sin^2\theta}}. \tag{A19}$$

Using these expressions, we can finally obtain the self-energy correction given by the Eqs. (10)–(13).

APPENDIX B: FERMION-DISORDER VERTEX CORRECTION DUE TO COULOMB INTERACTION

The correction to fermion-disorder vertex due to Coulomb interaction is given by

$$V_C = -\int \frac{d\Omega}{2\pi}\int \frac{d^2\mathbf{q}}{(2\pi)^2}\gamma_0 G_0(i\Omega,\mathbf{q})v_\Gamma\Gamma G_0(i\Omega,\mathbf{q})\gamma_0 \times V(\Omega,\mathbf{q}). \tag{B1}$$

One can impose a momentum cutoff by multiplying both fermion and boson propagators by a smooth function $\mathcal{K}(k^2/\Lambda^2)$, and then obtain

$$V_C = -v_\Gamma\int \frac{d^3Q}{(2\pi)^2}\gamma_0 G_0(Q)\Gamma G_0(Q)\gamma_0 V(Q)\mathcal{K}^3\left(\frac{\mathbf{q}^2}{\Lambda^2}\right). \tag{B2}$$

Therefore we have

$$\frac{dV_C}{d\ln\Lambda} = 6v_\Gamma\int \frac{d^3Q}{(2\pi)^3}\gamma_0 G_0(Q)\Gamma G_0(Q)\gamma_0 V(Q) \times \mathcal{K}^2\left(\frac{\mathbf{q}^2}{\Lambda^2}\right)\mathcal{K}'\left(\frac{\mathbf{q}^2}{\Lambda^2}\right)\left(\frac{\mathbf{q}^2}{\Lambda^2}\right). \tag{B3}$$

After converting to cylindrical coordinates defined by Eqs. (A8)–(A12), it is easy to get

$$\frac{dV_C}{d\Lambda} = v_\Gamma\frac{3v_1}{4\pi^3\Lambda}\int_{-\infty}^{+\infty}dx\int_0^{2\pi}d\theta\gamma_0 G(\hat{Q})\Gamma G(\hat{Q})\gamma_0 V(\hat{Q}) \times \int_0^{+\infty}dy y\mathcal{K}^2(y^2)\mathcal{K}'(y^2), \tag{B4}$$

where

$$\int_0^{+\infty}dy y\mathcal{K}^2(y^2)\mathcal{K}'(y^2) = -\frac{1}{6}. \tag{B5}$$

Finally, we obtain

$$\frac{dV_C}{d\ln\Lambda} = -v_\Gamma\frac{v_1}{8\pi^3}\int_{-\infty}^{+\infty}dx\int_0^{2\pi}d\theta H(\hat{Q}), \tag{B6}$$

where

$$H(\hat{Q}) = \gamma_0 G_0(\hat{Q})\Gamma G_0(\hat{Q})\gamma_0 V(\hat{Q}). \tag{B7}$$

APPENDIX C: SYMMETRIC FORM OF $C_{0,1,2}$ AND $\mathcal{G}$

The parameters $C_{0,1,2}$ and $\mathcal{G}$ appearing in RG equations can also be written in the following symmetric form:

$$C_0 = \frac{1}{8\pi^3}\int_0^{2\pi}d\theta\int_{-\infty}^{+\infty}dx \times \frac{x^2-(v_1/v_2)\cos^2\theta-(v_2/v_1)\sin^2\theta}{[x^2+(v_1/v_2)\cos^2\theta+(v_2/v_1)\sin^2\theta]^2}\mathcal{G}(x,\theta), \tag{C1}$$

$$C_1 = \frac{1}{8\pi^3}\int_0^{2\pi}d\theta\int_{-\infty}^{+\infty}dx \times \frac{x^2-(v_1/v_2)\cos^2\theta+(v_2/v_1)\sin^2\theta}{[x^2+(v_1/v_2)\cos^2\theta+(v_2/v_1)\sin^2\theta]^2}\mathcal{G}(x,\theta), \tag{C2}$$

$$C_2 = \frac{1}{8\pi^3}\int_0^{2\pi}d\theta\int_{-\infty}^{+\infty}dx \times \frac{x^2+(v_1/v_2)\cos^2\theta-(v_2/v_1)\sin^2\theta}{[x^2+(v_1/v_2)\cos^2\theta+(v_2/v_1)\sin^2\theta]^2}\mathcal{G}(x,\theta), \tag{C3}$$

with

$$\mathcal{G}^{-1}(x,\theta) = \frac{\epsilon\sqrt{v_1v_2}}{2\pi e^2}+\frac{N}{8} \times \frac{(v_1/v_2)\cos^2\theta+(v_2/v_1)\sin^2\theta}{\sqrt{x^2+(v_1/v_2)\cos^2\theta+(v_2/v_1)\sin^2\theta}}. \tag{C4}$$

The expressions for $C_{0,1,2}$ and $\mathcal{G}$ shown in Eqs. (C1)–(C4) are indeed equivalent to those in Eqs. (11)–(14).

APPENDIX D: DERIVATION FOR THE DIFFERENTIAL EQUATIONS OF DOS AND SPECIFIC HEAT

We now study the influence of Coulomb interaction on DOS using the method employed by Xu *et al.* [25]. The DOS $\rho(\omega)$ is defined as

$$\rho(\omega) = N\int\frac{dk_1dk_2}{(2\pi)^2}\mathrm{Tr}\{\mathrm{Im}[G^R(\omega,v_1k_1,v_2k_2)]\} = \frac{N}{v_1v_2}\int\frac{dk_1'dk_2'}{(2\pi)^2}\mathrm{Tr}\{\mathrm{Im}[G^R(\omega,k_1',k_2')]\}, \tag{D1}$$

where $G^R(\omega,k_1,k_2)$ is the retarded propagator of Dirac fermions. According to the method in Xu *et al.* [25], DOS $\rho(\omega)$ and specific heat $C_V(T)$ can be calculated through the differential equations $\frac{d\ln\rho}{d\ln\omega}$ and $\frac{d\ln C_V}{d\ln T}$, respectively. The qualitative behavior of $\rho(\omega)$ is related to both the fermion anomalous dimension, $\eta_f = -C_0+C_g$, and the dynamical exponents $z_{1,2}$, which are encoded in the flow of fermion velocities $v_{1,2}$. However, the qualitative behavior of $C_V(T)$ is only related to the dynamical exponents $z_{1,2}$. Therefore one should represent $\frac{d\ln\rho}{d\ln\omega}$ in terms of the fermion anomalous dimension η_f and the RG equations of $v_{1,2}$, but express $\frac{d\ln C_V}{d\ln T}$ only through the RG equations of $v_{1,2}$. In Sec. III B, we have obtained the l dependence of the RG equations of $v_{1,2}$, as well as $C_{0,g}$. In order to get $\frac{d\ln\rho}{d\ln\omega}$ and $\frac{d\ln C_V}{d\ln T}$, we need to replace $\frac{d}{d\ln\omega}$ or $\frac{d}{d\ln T}$ with $\frac{d}{dl}$.

At a certain given energy ω, the corresponding momentum scale should be determined by the larger component of the fermion velocities [25], namely,

$$\tilde{p} = \frac{\omega}{\max(v_1,v_2)}, \tag{D2}$$

which leads to

$$\frac{d\ln\omega}{d\ln\tilde{p}} = 1+\frac{d\ln\max(v_1,v_2)}{d\ln\tilde{p}}. \tag{D3}$$

Now the scaling equation for $\rho(\omega)$ takes the form

$$\frac{d\ln\rho}{d\ln\omega} = \frac{d\ln\rho}{d\ln\tilde{p}\frac{d\ln\omega}{d\ln\tilde{p}}} = \frac{d\ln\rho}{d\ln\tilde{p}\left[1+\frac{d\ln\max(v_1,v_2)}{d\ln\tilde{p}}\right]}. \tag{D4}$$

Since $\tilde{p} \sim \Lambda e^{-l}$, which leads to $d\ln\tilde{p} \sim -dl$, we can get

$$\frac{d\ln\rho}{d\ln\omega} = -\frac{d\ln\rho}{dl\left[1-\frac{d\ln\max(v_1,v_2)}{dl}\right]}, \tag{D5}$$

namely

$$\frac{d\ln\rho}{d\ln\omega} = -\frac{-(1+C_0-C_g)+\frac{d\ln\left(\frac{1}{v_1v_2}\right)}{dl}}{\left[1-\frac{d\ln\max(v_1,v_2)}{dl}\right]}. \tag{D6}$$

The first term $-(1+C_0-C_g)$ in the numerator comes form the scaling exponent of the fermion propagator in Eq. (D1). The second term $d\ln(\frac{1}{v_1v_2})/dl$ is induced by the prefactor $\frac{1}{v_1v_2}$ in Eq. (D1). Equation (D6) can be further written as

$$\frac{d\ln\rho}{d\ln\omega} = \frac{1+C_0-C_g+\frac{d\ln v_1}{dl}+\frac{d\ln v_2}{dl}}{\left[1-\frac{d\ln\max(v_1,v_2)}{dl}\right]}. \tag{D7}$$

Using the RG equations of v_1 and v_2, i.e., Eqs. (46) and (47), the above equation can be simplified to

$$\frac{d\ln\rho}{d\ln\omega} = \frac{1+3C_0-C_1-C_2-3C_g}{1-C_0+C_1+C_g} \tag{D8}$$

for $v_1 > v_2$, and

$$\frac{d\ln\rho}{d\ln\omega} = \frac{1+3C_0-C_1-C_2-3C_g}{1-C_0+C_2+C_g} \tag{D9}$$

for $v_2 > v_1$.

To calculate the specific heat, we also follow the method used in Ref. [25]. The free energy $\mathcal{F} = T\ln\mathcal{Z}/V$ contains the following singular part:

$$\mathcal{F} = (\xi_\tau\xi_x\xi_y)^{-1}, \tag{D10}$$

where $\xi_\tau \sim 1/T$, $\xi_x \sim v_1\xi_\tau$, and $\xi_y \sim v_2\xi_\tau$. In an interacting anisotropic graphene, the free energy if found to behave like

$$\mathcal{F} \sim \frac{1}{v_1v_2}T^3. \tag{D11}$$

The corresponding specific heat is given by

$$C_V = -T\frac{\partial^2\mathcal{F}}{\partial T^2} \sim \frac{1}{v_1v_2}T^2. \tag{D12}$$

After taking differentiation with respect to T, we get

$$\frac{d\ln C_V}{d\ln T} = 2+\frac{d\ln\left(\frac{1}{v_1v_2}\right)}{d\ln T}. \tag{D13}$$

At certain given temperature T, the corresponding momentum scale should be determined by the larger component of the fermion velocities as [25]

$$\tilde{p} = \frac{T}{\max(v_1,v_2)}, \tag{D14}$$

which leads to

$$\frac{d\ln T}{d\ln\tilde{p}} = 1+\frac{d\ln\max(v_1,v_2)}{d\ln\tilde{p}}. \tag{D15}$$

Now the scaling equation for C_V becomes

$$\begin{aligned}\frac{d\ln C_V}{d\ln T} &= 2+\frac{d\ln\left(\frac{1}{v_1v_2}\right)}{d\ln\tilde{p}\frac{d\ln T}{d\ln\tilde{p}}}\\ &= 2+\frac{d\ln\left(\frac{1}{v_1v_2}\right)}{d\ln\tilde{p}\left[1+\frac{d\ln\max(v_1,v_2)}{d\ln\tilde{p}}\right]}.\end{aligned} \tag{D16}$$

Using the expression $d\ln\tilde{p} \sim -dl$, it is easy to get

$$\begin{aligned}\frac{d\ln C_V}{d\ln T} &= 2-\frac{d\ln\left(\frac{1}{v_1v_2}\right)}{dl\left[1-\frac{d\ln\max(v_1,v_2)}{dl}\right]}\\ &= 2+\frac{\frac{d\ln v_1}{dl}+\frac{d\ln v_2}{dl}}{\left[1-\frac{d\ln\max(v_1,v_2)}{dl}\right]}.\end{aligned} \tag{D17}$$

After substituting Eqs. (46) and (47) into (D17), we finally obtain

$$\frac{d\ln C_V}{d\ln T} = 2+\frac{2C_0-C_1-C_2-2C_g}{1-C_0+C_1+C_g} \tag{D18}$$

for $v_1 > v_2$, and

$$\frac{d\ln C_V}{d\ln T} = 2+\frac{2C_0-C_1-C_2-2C_g}{1-C_0+C_2+C_g} \tag{D19}$$

for $v_2 > v_1$.

APPENDIX E: DIFFERENT DEPENDENCE OF DOS AND SPECIFIC HEAT ON A POSITIVE ANOMALOUS DIMENSION

In this Appendix, we would like to demonstrate the different influence of a finite positive anomalous dimension on DOS and specific heat. This may help us to understand the results obtained in Secs. V B and V C. For this purpose, it is convenient to consider a generic model of interacting Dirac fermions.

Let us start from a free Dirac fermion propagator with an isotropic dispersion,

$$G_0(i\omega_n,\mathbf{k}) = \frac{1}{i\omega_n\gamma_0-v_F\gamma\cdot\mathbf{k}} = \frac{-i\omega_n\gamma_0+v_F\gamma\cdot\mathbf{k}}{\omega_n^2+v_F^2k^2}, \tag{E1}$$

where $\omega_n = (2n+1)\pi T$ is the Matsubara frequency. Carrying out analytic continuation $i\omega_n \to \omega+i\delta$, we can get the retarded propagator

$$\begin{aligned}G_0^R(\omega,\mathbf{k}) = &\left[\mathcal{P}\frac{1}{\omega^2-v_F^2k^2}-i\pi\,\mathrm{sgn}(\omega)\delta\left(\omega^2-v_F^2k^2\right)\right]\\ &\times(\omega\gamma_0-v_F\gamma\cdot\mathbf{k}).\end{aligned} \tag{E2}$$

From this propagator, it is easy to get a spectral function

$$\begin{aligned}A_0(\omega,\mathbf{k}) &= -\frac{1}{\pi}\mathrm{Tr}\left[\gamma_0\mathrm{Im}G_0^R(\omega,\mathbf{k})\right]\\ &= 2\left[\delta\left(v_Fk-|\omega|\right)+\delta\left(v_Fk+|\omega|\right)\right].\end{aligned} \tag{E3}$$

The fermion DOS can be computed directly, i.e.,

$$\rho_0(\omega) = N\int\frac{d^2\mathbf{k}}{(2\pi)^2}A_0(\omega,\mathbf{k}) = \frac{N}{\pi v_F^2}|\omega|. \tag{E4}$$

The free energy for free fermions is therefore

$$F_0(T) = 4NT\sum_{\omega_n}\int \frac{d^2\mathbf{k}}{(2\pi)^2}\ln\left[\left(\omega_n^2+v_F^2k^2\right)^{\frac{1}{2}}\right] = 2N\int\frac{d^2k}{(2\pi)^2}T\sum_{\omega_n}\ln\left[\omega_n^2+v_F^2k^2\right]. \quad \text{(E5)}$$

The summation over frequency ω_n can be easily performed, leading to

$$F_0(T) = 2N\int\frac{d^2\mathbf{k}}{(2\pi)^2}\left[v_Fk - 2T\ln\left(1+e^{-\frac{v_Fk}{T}}\right)\right], \quad \text{(E6)}$$

which is clearly divergent. In order to get a finite free energy, we redefine $F_0(T)-F_0(0)$ as $F_0(T)$ and get

$$F_0(T) = -4NT\int\frac{d^2\mathbf{k}}{(2\pi)^2}\ln\left[1+e^{-\frac{v_Fk}{T}}\right] = -\frac{3N\zeta(3)}{2\pi v_F^2}T^3. \quad \text{(E7)}$$

The corresponding specific heat is

$$C_{V0} = -T\frac{\partial^2F_0(T)}{\partial T^2} = \frac{9N\zeta(3)}{\pi v_F^2}T^2. \quad \text{(E8)}$$

Now suppose the fermion propagator acquires a finite positive anomalous dimension η due to some interaction [19,85,88,89], yielding

$$G(i\omega_n,\mathbf{k}) = \frac{1}{(i\omega_n\gamma_0 - v_F\gamma\cdot\mathbf{k})\left(\frac{\sqrt{\omega_n^2+v_F^2k^2}}{v_F\Lambda}\right)^{-\eta}} = \frac{-(i\omega_n\gamma_0 - v_F\gamma\cdot\mathbf{k})}{(v_F\Lambda)^\eta\left(\omega_n^2+v_F^2k^2\right)^{1-\frac{\eta}{2}}}. \quad \text{(E9)}$$

The retarded propagator is therefore given by

$$G^R(\omega,\mathbf{k}) = \theta(v_Fk-|\omega|)\left[\mathcal{P}\frac{1}{\omega^2-v_F^2k^2} - i\pi\,\mathrm{sgn}(\omega)\delta\left(\omega^2-v_F^2k^2\right)\right]\frac{(\omega\gamma_0 - v_F\gamma\cdot\mathbf{k})}{(v_F\Lambda)^\eta\left(\sqrt{v_F^2k^2-\omega^2}\right)^{-\eta}}$$
$$+\theta(|\omega|-v_Fk)\left[\mathcal{P}\frac{1}{\omega^2-v_F^2k^2} - i\pi\,\mathrm{sgn}(\omega)\delta\left(\omega^2-v_F^2k^2\right)\right]\frac{(\omega\gamma_0 - v_F\gamma\cdot\mathbf{k})}{(v_F\Lambda)^\eta\left(\sqrt{\omega^2-v_F^2k^2}\right)^{-\eta}}$$
$$\times\left[\cos\left(\frac{\pi\eta}{2}\right) - \mathrm{sgn}(\omega)i\sin\left(\frac{\pi\eta}{2}\right)\right], \quad \text{(E10)}$$

which results in the following spectral function:

$$A(\omega,\mathbf{k}) = -\frac{1}{\pi}\mathrm{Tr}[\gamma_0\mathrm{Im}G^R(\omega,\mathbf{k})] = \frac{4}{\pi}\frac{\theta(|\omega|-v_Fk)|\omega|\sin\left(\frac{\pi\eta}{2}\right)}{(v_F\Lambda)^\eta\left(\sqrt{\omega^2-v_F^2k^2}\right)^{2-\eta}}. \quad \text{(E11)}$$

Now the fermion DOS depends on η as

$$\rho(\omega) = N\int\frac{d^2\mathbf{k}}{(2\pi)^2}A(\omega,\mathbf{k}) = \frac{2N}{\pi^2}\frac{1}{\eta}\sin\left(\frac{\pi\eta}{2}\right)\frac{|\omega|^{1+\eta}}{v_F^2(v_F\Lambda)^\eta}, \quad \text{(E12)}$$

where η modifies the ω dependence of $\rho(\omega)$. However, the free energy of interacting fermions is

$$F(T) = 4NT\sum_{\omega_n}\int\frac{d^2\mathbf{k}}{(2\pi)^2}\ln\left[\left(\omega_n^2+v_Fk^2\right)^{\frac{1}{2}-\frac{\eta}{2}}\right] = (1-\eta)\,2N\int\frac{d^2k}{(2\pi)^2}T\sum_{\omega_n}\ln\left[\omega_n^2+v_F^2k^2\right]. \quad \text{(E13)}$$

$$= (1-\eta)\,2N\int\frac{d^2\mathbf{k}}{(2\pi)^2}\left[v_Fk - 2T\ln\left(1+e^{-\frac{v_Fk}{T}}\right)\right], \quad \text{(E14)}$$

which is also divergent. Similar to Eq. (E7), the finite redefined $F(T)$ has the form

$$F(T) = -(1-\eta)\,4NT\int\frac{d^2\mathbf{k}}{(2\pi)^2}\ln\left[1+e^{-\frac{v_Fk}{T}}\right] = -(1-\eta)\frac{3N\zeta(3)}{2\pi v_F^2}T^3, \quad \text{(E15)}$$

which leads to the specific heat

$$C_V = -T\frac{\partial^2F(T)}{\partial T^2} = (1-\eta)\frac{9N\zeta(3)}{\pi v_F^2}T^2. \quad \text{(E16)}$$

Comparing Eq. (E4) with Eq. (E12), we see that the fermion DOS is linear in energy for the free system, but the linear dependence on energy of DOS is changed once a finite positive anomalous dimension η is generated in the fermion propagator [90,91]. The quadratic T dependence of specific heat does not change even if $\eta\neq 0$ [85,91,92]. From Eq. (E16), we see that η enters into the specific heat only in the prefactor of T^2.

Now let us go back to the interacting model considered in this paper. Due to the interplay of Coulomb interaction and a random gauge potential (random mass), the fermion DOS is no longer linear in ω in the limit $\omega\to 0$, but the specific heat still exhibits quadratic T dependence in the limit $T\to 0$. The reason for this behavior is that the fermion velocities

v_1 and v_2 approach a constant at the lowest energy, which means the dynamical exponent $z \to 1$, whereas the fermion propagator acquires a finite positive anomalous dimension $\eta = \lim_{l\to\infty}[-C_0(l) + C_g(l)]$.

[1] P. A. Lee, N. Nagaosa, and X.-G. Wen, Rev. Mod. Phys. **78**, 17 (2006).
[2] J. Orenstein and A. J. Millis, Science **288**, 468 (2000).
[3] M. Z. Hasan and C. L. Kane, Rev. Mod. Phys. **82**, 3045 (2010).
[4] K. S. Novoselov, A. K. Geim, S. V. Morozov, D. Jiang, Y. Zhang, S. V. Dubonos, I. V. Grigorieva, and A. A. Firsov, Science **306**, 666 (2004).
[5] K. S. Novoselov, A. K. Geim, S. V. Morozov, D. Jiang, M. I. Katsnelson, I. V. Grigorieva, S. V. Dubonos, and A. A. Firsov, Nature (London) **438**, 197 (2005).
[6] A. H. Castro Neto, F. Guinea, N. M. R. Peres, K. S. Novoselov, and A. K. Geim, Rev. Mod. Phys. **81**, 109 (2009).
[7] N. M. R. Peres, Rev. Mod. Phys. **82**, 2673 (2010).
[8] S. Das Sarma, S. Adam, E. H. Hwang, and E. Rossi, Rev. Mod. Phys. **83**, 407 (2011).
[9] V. N. Kotov, B. Uchoa, V. M. Pereira, F. Guinea, and A. H. Castro Neto, Rev. Mod. Phys. **84**, 1067 (2012).
[10] V. M. Pereira, A. H. Castro Neto, and N. M. R. Peres, Phys. Rev. B **80**, 045401 (2009).
[11] R. M. Ribeiro, V. M. Pereira, N. M. R. Peres, P. R. Briddon, and A. H. Castro Neto, New J. Phys. **11**, 115002 (2009).
[12] M. O. Goerbig, J.-N. Fuchs, G. Montambaux, and F. Piéchon, Phys. Rev. B **78**, 045415 (2008).
[13] S.-M. Choi, S.-H. Jhi, and Y-W. Son, Phys. Rev. B **81**, 081407(R) (2010).
[14] C.-H. Park, L. Yang, Y.-W. Son, M. L. Cohen, and S. G. Louie, Nat. Phys. **4**, 213 (2008).
[15] C.-H. Park, L. Yang, Y.-W. Son, M. L. Cohen, and S. G. Louie, Phys. Rev. Lett. **101**, 126804 (2008).
[16] S. Rusponi, M. Papagno, P. Moras, S. Vlaic, M. Etzkorn, P. M. Sheverdyaeva, D. Pacilé, H. Brune, and C. Carbone, Phys. Rev. Lett. **105**, 246803 (2010).
[17] M. Franz and Z. Tešanović, Phys. Rev. Lett. **87**, 257003 (2001).
[18] O. Vafek, Z. Tešanović, and M. Franz, Phys. Rev. Lett. **89**, 157003 (2002).
[19] M. Franz, Z. Tešanović, and O. Vafek, Phys. Rev. B **66**, 054535 (2002).
[20] I. F. Herbut, Phys. Rev. B **66**, 094504 (2002).
[21] D. J. Lee and I. F. Herbut, Phys. Rev. B **66**, 094512 (2002).
[22] M. Hermele, T. Senthil, and M. P. A. Fisher, Phys. Rev. B **72**, 104404 (2005).
[23] E.-A. Kim, M. J. Lawler, P. Oreto, S. Sachdev, E. Fradkin, and S. A. Kivelson, Phys. Rev. B **77**, 184514 (2008).
[24] Y. Huh and S. Sachdev, Phys. Rev. B **78**, 064512 (2008).
[25] C. Xu, Y. Qi, and S. Sachdev, Phys. Rev. B **78**, 134507 (2008).
[26] L. Fritz and S. Sachdev, Phys. Rev. B **80**, 144503 (2009).
[27] J. Wang, G.-Z. Liu, and H. Kleinert, Phys. Rev. B **83**, 214503 (2011).
[28] G.-Z. Liu, J.-R. Wang, and J. Wang, Phys. Rev. B **85**, 174525 (2012).
[29] J. Wang and G.-Z. Liu, New J. Phys. **15**, 073039 (2013).
[30] A. Pelissetto, S. Sachdev, and E. Vicari, Phys. Rev. Lett. **101**, 027005 (2008).
[31] R. Shankar, Rev. Mod. Phys. **66**, 129 (1994).
[32] A. Sharma, V. N. Kotov, and A. H. Castro Neto, arXiv:1206.5427.
[33] A. W. W. Ludwig, M. P. A. Fisher, R. Shankar, and G. Grinstein, Phys. Rev. B **50**, 7526 (1994); A. A. Nersesyan, A. M. Tsvelik, and F. Wenger, Nucl. Phys. B **438**, 561 (1995); C. Mudry, C. Chamon, and X.-G. Wen, *ibid.* **466**, 383 (1996); A. Altland, B. D. Simons, and M. R. Zirnbauer, Phys. Rep. **359**, 283 (2002).
[34] T. Stauber, F. Guinea, and M. A. H. Vozmediano, Phys. Rev. B **71**, 041406(R) (2005).
[35] I. F. Herbut, V. Juričić, and O. Vafek, Phys. Rev. Lett. **100**, 046403 (2008).
[36] O. Vafek and M. J. Case, Phys. Rev. B **77**, 033410 (2008).
[37] D. V. Khveshchenko, Phys. Rev. Lett. **87**, 246802 (2001).
[38] E. V. Gorbar, V. P. Gusynin, V. A. Miransky, and I. A. Shovkovy, Phys. Rev. B **66**, 045108 (2002).
[39] D. V. Khveshchenko and H. Leal, Nucl. Phys. B **687**, 323 (2004).
[40] G.-Z. Liu, W. Li, and G. Cheng, Phys. Rev. B **79**, 205429 (2009).
[41] D. V. Khveshchenko, J. Phys.: Condens. Matter **21**, 075303 (2009).
[42] O. V. Gamayun, E. V. Gorbar, and V. P. Gusynin, Phys. Rev. B **81**, 075429 (2010).
[43] S. Hands and C. Strouthos, Phys. Rev. B **78**, 165423 (2008).
[44] J. E. Drut and T. A. Lähde, Phys. Rev. Lett. **102**, 026802 (2009); Phys. Rev. B **79**, 165425 (2009); **79**, 241405(R) (2009).
[45] A. H. Castro Neto, Physics **2**, 30 (2009).
[46] C.-X. Zhang, G.-Z. Liu, and M.-Q. Huang, Phys. Rev. B **83**, 115438 (2011).
[47] G.-Z. Liu and J.-R. Wang, New J. Phys. **13**, 033022 (2011).
[48] J.-R. Wang and G.-Z. Liu, New J. Phys. **14**, 043036 (2012).
[49] J. Gonzalez, F. Guinea, and M. A. H. Vozmediano, Mod. Phys. Lett. B **7**, 1593 (1993); Nucl. Phys. B **424**, 595 (1994).
[50] J. Gonzalez, F. Guinea, and M. A. H. Vozmediano, Phys. Rev. B **59**, 2474(R) (1999).
[51] D. T. Son, Phys. Rev. B **75**, 235423 (2007).
[52] O. Vafek, Phys. Rev. Lett. **98**, 216401 (2007).
[53] D. E. Sheehy and J. Schmalian, Phys. Rev. Lett. **99**, 226803 (2007).
[54] E. H. Hwang, BenYu-Kuang Hu, and S. Das Sarma, Phys. Rev. Lett. **99**, 226801 (2007).
[55] L. Fritz, J. Schmalian, M. Müller, and S. Sachdev, Phys. Rev. B **78**, 085416 (2008).
[56] E. G. Mishchenko, Europhys. Lett. **83**, 17005 (2008).
[57] D. E. Sheehy and J. Schmalian, Phys. Rev. B **80**, 193411 (2009).
[58] V. Juričić, O. Vafek, and I. F. Herbut, Phys. Rev. B **82**, 235402 (2010).
[59] V. N. Kotov, B. Uchoa, and A. H. Castro Neto, Phys. Rev. B **78**, 035119 (2008).
[60] I. Sodemann and M. M. Fogler, Phys. Rev. B **86**, 115408 (2012).
[61] B. Rosenstein, M. Lewkowicz, and T. Maniv, Phys. Rev. Lett. **110**, 066602 (2013).

[62] G. Gazzola, A. L. Cherchiglia, L. A. Cabral, M. C. Nemes, and M. Sampaio, Europhys. Lett. **104**, 27002 (2013).
[63] D. C. Elias, R. V. Gorbachev, A. S. Mayorov, S. V. Morozov, A. A. Zhukov, P. Blake, L. A. Ponomarenko, I. V. Grigorieva, K. S. Novoselov, F. Guinea, and A. K. Geim, Nat. Phys. **7**, 701 (2011).
[64] G. L. Yu, R. Jalil, B. Belle, A. S. Mayorov, P. Blake, F. Schedin, S. V. Morozov, L. A. Ponomarenko, F. Chiappini, S. Wiedmann, U. Zeitler, M. I. Katsnelson, A. K. Geim, K. S. Novoselov, and D. C. Elias, Proc. Natl. Acad. Sci. USA **110**, 3282 (2013).
[65] D. A. Siegel, C.-H. Park, C. Hwang, J. Deslippe, A. V. Fedorov, S. G. Louie, and A. Lanzara, Proc. Natl. Acad. Sci. USA **108**, 11365 (2012).
[66] E. R. Mucciolo and C. H. Lewenkopf, J. Phys.: Condens. Matter **22**, 273201 (2010).
[67] J. C. Meyer, A. K. Geim, M. I. Katsnelson, K. S. Novoselov, T. J. Booth, and S. Roth, Nature (London) **446**, 60 (2007).
[68] T. Champel and S. Florens, Phys. Rev. B **82**, 045421 (2010).
[69] S. Viola Kusminskiy, D. K. Campbell, A. H. Castro Neto, and F. Guinea, Phys. Rev. B **83**, 165405 (2011).
[70] F. M. D. Pellegrino, G. G. N. Angilella, and R. Pucci, Phys. Rev. B **84**, 195407 (2011).
[71] J. P. F. LeBlanc and J. P. Carbotte, Phys. Rev. B **87**, 205407 (2013).
[72] A. Sharma, V. N. Kotov, and A. H. Castro Neto, Phys. Rev. B **87**, 155431 (2013).
[73] I. L. Aleiner, D. E. Kharzeev, and A. M. Tsvelik, Phys. Rev. B **76**, 195415 (2007).
[74] J. A. Hertz, Phys. Rev. B **14**, 1165 (1976).
[75] H. v. Löhneysen, A. Rosch, M. Vojta, and P. Wölfle, Rev. Mod. Phys. **79**, 1015 (2007).
[76] I. F. Herbut, *A Modern Approach to Critical Phenomena* (Cambriage University Press, Cambriage, UK, 2007).
[77] M. A. Cotinentino, *Quantum Scaling in Many-Body Systems* (World Scientific Press, Singapore, 2001).
[78] Y. Nambu and G. Jona-Lasinio, Phys. Rev. **122**, 345 (1961).
[79] V. A. Miransky, *Dynamical Symmetry Breaking in Quantum Field Theories* (World Scientific, Singapore, 1993).
[80] C. D. Roberts and S. M. Schmidt, Prog. Part. Nucl. Phys. **45**, S1 (2000).
[81] A. K. Geim and K. S. Novoselov, Nat. Mater. **6**, 183 (2007).
[82] A. S. Mayorov, D. C. Elias, I. S. Mukhin, S. V. Morozov, L. A. Ponomarenko, K. S. Novoselov, A. K. Geim, and R. V. Gorbachev, Nano Lett. **12**, 4629 (2012).
[83] J.-R. Wang and G.-Z. Liu, New J. Phys. **15**, 063007 (2013).
[84] I. F. Herbut, Phys. Rev. Lett. **97**, 146401 (2006).
[85] I. F. Herbut, V. Juričić, and B. Roy, Phys. Rev. B **79**, 085116 (2009).
[86] B. Roy and I. F. Herbut, Phys. Rev. B **82**, 035429 (2010).
[87] B. Roy, V. Juričić, and I. F. Herbut, Phys. Rev. B **87**, 041401 (2013).
[88] D. V. Khveshchenko and J. Paaske, Phys. Rev. Lett. **86**, 4672 (2001).
[89] S. Sachdev, arXiv:1012.0299v5.
[90] V. P. Gusynin, D. V. Khveshchenko, and M. Reenders, Phys. Rev. B **67**, 115201 (2003).
[91] Y. Zhong, K. Liu, Y.-Q. Wang, and H.-G. Luo, Phys. Rev. B **86**, 165134 (2012).
[92] R. K. Kaul and S. Sachdev, Phys. Rev. B **77**, 155105 (2008).